2012

# An experimental and theoretical critique of flow model accuracy

Shannon Ray Chollett
*Louisiana State University and Agricultural and Mechanical College*, scholl1@lsu.edu

# AN EXPERIMENTAL AND THEORETICAL CRITIQUE OF FLOW MODEL ACCURACY

A Thesis
Submitted to the Graduate Faculty of the
Louisiana State University and
Agricultural and Mechanical College
in partial fulfillment of the
requirements for the degree of
Master of Science in Petroleum Engineering
in
The Department of Petroleum Engineering

by
Shannon Ray Chollett
B.S. Geophysics, Boise State University 2009
May 2012

# Acknowledgements

I would like to thank my committee, Dr. Christopher White, Dr. Juan Lorenzo, and Dr. Mayank Tyagi, for their guidance throughout my graduate career. My committee was always willing to discuss ideas and questions. I also would like to thank David Smolkin for his guidance using the seismic data collection equipment. I would like to give a special thanks to Ting Sun for helping me with technical computing problems. I am very grateful to for the UCoMS group meetings and all that was discussed and encouraged there. The knowledge and experience gained there helped me overcome many issues while performing experiments in the wave tank. I would also like to thank Dr. Gregory Stone for allowing me to use the wave tank at LSU. I would like to thank Dr. John Smith for accepting me as a student in my first semester at LSU. Dr. Smith took me under his supervision and helped me get started in Grad School. Without him I would not have been able to study at LSU. I would also like to thank the Department of Energy, research agreement DOE/LEQSF(2004-7)-L, and the Shell E&P Technology Company who provided the monetary support for this project. Because of their assistance, I was able to complete my master's degree. Finally, I would like to that all of my friends and family for their support during the last 2 plus years, especially my beautiful wife Shannon.

# Table of Contents

# List of Figures

# Abstract

In today's exploration and production environment it is required that engineers must collect and use vast amounts of data for flow model construction and calibration, as well as reservoir estimation and optimization. With modern technology, the data volume can be overwhelming. It is necessary that data monitoring and calibration are highly efficient. It is also essential that physical and mathematical models can be tested in repeatable, inexpensive experiments. The experiments described in this thesis will develop and perform verification of algorithms and can generate prior geomodels, collect and process seismic refraction data, collect and process production data, and calibrate these models.

The experimental components discussed here are collectively referred to as *The Sand Tank Experiment*. Contained in the LSU WaveCIS tank is a wedge shaped sand pack that can be saturated with water. Water can then be produced from this model reservoir while it is monitored by pressure/temperature sensors. A 20 kHz seismic source and 8 accelerometers are used to collect seismic first arrival data during this production period. This data can then be used to image varying water saturations throughout the reservoir. Those water saturations modify the compressional, p-wave, seismic velocities as described in the Biot and Gassman relationships. Picking first arrival times for each run of the experiment can further enhance the use of the seismic data. These first arrival times can then be compared to calculated first arrival times from simulation data and the residuals can be used to measure the accuracy.

# Chapter 1

# Introduction

## 1.1 Background

For years, flow models have been used to explain the flow of fluids in porous media. Recently, numerical models have been used to predict and analyze porous media flow, especially if the problems under consideration are nonlinear or have spatial heterogeneity. Five approaches have been widely used: pore network models, lattice gas and lattice Boltzmann methods, Monte Carlo methods, particle methods (molecular dynamics, dissipative particle dynamics, and smoothed particle hydrodynamics), and conventional grid-based computational fluid dynamics coupled with interface tracking and a contact angle models (Meakin and Tartakovsky 2009). While all of these methods are well proven scientific methods that achieve correct results when used with care, all of them are prone to error and may give incorrect predictions; even the best fluid flow or reservoir simulators have assumptions and limitations. A complex model may be more realistic, yet ironically, as we add more factors to a model, the certainty of its predictions may decrease even as our intuitive faith in the model increases. For this and other reasons, model output should not be viewed as an accurate prediction of the future state of the system (Oreskes 2003).

One way to check the accuracy of these flow models is to compare them to observed responses. Large scale projects in the field can provide data for flow models and history matching algorithms, but they are expensive, both in time and money. Data is sparse and sometimes unreliable. If only there were a way to make several inexpensive large scale flow models, while being able to compare them to several inexpensive robust datasets.

## 1.2 Motivation

As previously mentioned, there is no accurate way to model fluid flow in porous media that is not prone to error. Furthermore, trying to predict future flow behavior is even harder. Models of natural systems can never fully specify the systems

that they describe, and therefore their predictions are always subject to uncertainties that we cannot fully specify (Oreskes 2003). The proposition is to make flow models more accurate by comparing them to actual production data collected in a controlled environment; that could be changed to mimic different situations. Observations would be collected in an environment that was safe and easy to manipulate. Several repeatable experiments could be run using the exact same interpretation and analysis techniques. Not only would time and money be saved, but the number of data and the number of configurations to your physical model are virtually endless and left up to the imagination of the engineer. A virtual data warehouse could be created with hundreds and even thousands of simulations with actual production data to compare the results to.

## 1.3 Experimental Description

The experiments are being performed in the Wave-CIS tank in the Geology building here at Louisiana State University. Contained in the Wave tank is a heterogenous sand pack as pictured in figure 1.1. This wedge shaped sand pack measures approximately $6 \times 9 \times 0.6$ m and can be filled to any depth desired with water. This wave tank is commonly referred to as the *sand tank*. Currently, up to five wells can be placed anywhere in the sand tank and water will be produced from one while the other wells will act as monitoring wells for the experiment. Each well is lined with slotted PVC pipe so that water can pass through freely and serve as a sink, analogous to a well in the subsurface. Pressure and temperature measurements can be monitored at each well location along with one measurement in the open water (which provides a time–varying boundary condition for the flow models). Production rate is also measured and controlled. A 20 kHz seismic source, along with 8 accelerometer receivers, are used to collect seismic refraction and reflection data to image varying degrees of water saturation within the sand tank. Those water saturations modify the compressional, p-wave, seismic velocities as described in the work of Biot (1956b) and Gassmann (1951).

Once the production and seismic data are collected and processed, first break picks can be made and forwarded to the inversion process. The model inversion in this experiment is done using a parallel implementation of an Ensemble Kalman Filter, more commonly referred to as EnKF. The inversion process then creates velocity models from water saturation levels provided by simulation data to calculate synthetic arrival times. The inversion process calculates arrival times from matching velocity models using a ray tracing algorithm known as rayinvr (Zelt 1988). After the ray tracing program has been run, the process compares the synthetic arrival times with experimentally collected arrival times.

Flow simulation is provided by CMG (Computer Modeling Group LTD.) reservoir simulation software and a reservoir simulator developed at LSU called BlackOil (El-Khamra 2009). This simulator is designed to scale on shared memory and can handle the unusual boundary conditions in the sand tank. A schematic from Black-

Oil (Fig. 1.1) shows the reservoir shape, locations of monitoring wells, and seismic survey line.

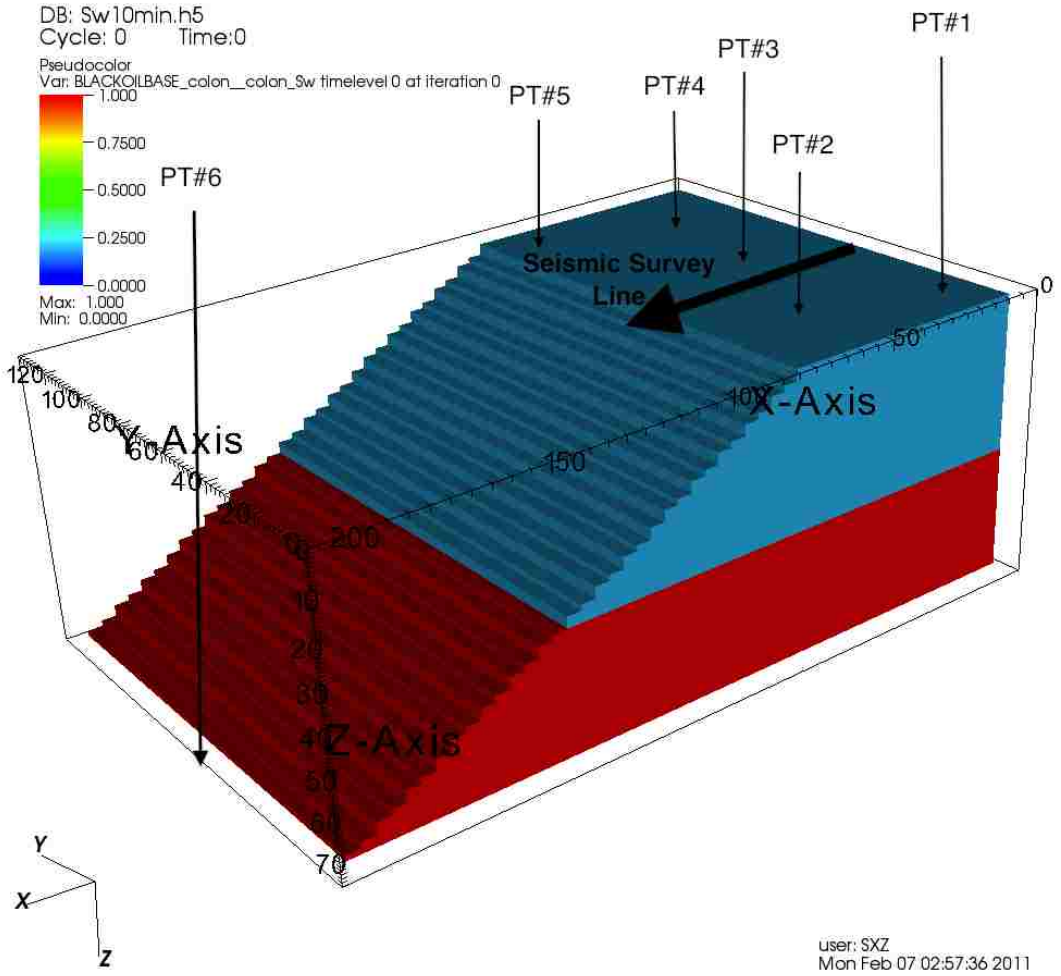


Figure 1.1: Sand tank schematic. Pictured above is a 3-D schematic of the sand tank as seen in the black oil simulator. The colors are describing water saturation in the tank at an initial condition. For simulation purposes the tank is broken up into 3-D grid blocks so that properties can be different inside each individual block. The locations of the five observation wells with pressure and temperature sensors are shown as PT#X, with a sixth sensor in the free water end of the tank. Note the location of sensor PT#3 is the production well from which water is being pumped from the tank. Also notice the location of the seismic survey line on which eight different shots from the 20 kHz seismic source with be collected by an array of eight accelerometers, for a total of sixty four seismic traces.

## 1.4 Key Points

- The value of model predictions is undermined by their uncertainty, which arises primarily from the fact that our models of complex natural systems are always open. Moreover, the attempt to make models capture the complexities of natural systems leads to a paradox: the more we strive for realism by incorporating as many as possible of the different processes and parameters that we believe to be operating in the system, the more difficult it is for us to know if our tests of the model are meaningful (Oreskes 2003).

- The accuracy of these models can be quantified and calibrated using real field data but that is costly.

- The experiment being conducted here is collecting observation data such as production rate and pressure change over time. This data is comparable to production data encountered in real world reservoir estimation cases.

# Chapter 2

# Background for Experimental Measurements

## 2.1 Geophysical Theory

The velocities of various types of seismic waves in homogenous, isotropic, elastic media are given by Mavko, Mukerji, and Dvorkin (1998).

$$V_P = \sqrt{\frac{K + \frac{4}{3}\mu}{\rho}}$$

$$V_S = \sqrt{\frac{\mu}{\rho}}$$

Where $V_P$ is the compressional wave velocity, $V_S$ is the shear wave velocity, $\rho$ is the density, $K$ is the bulk modulus, and $\mu$ is the shear modulus.

The general linear stress-strain relations for a porous elastic solid with fluid were derived by Biot (Biot 1956b; Biot 1956a; Biot 1962). At its low frequency limit, Biot's theory relates saturated elastic constants to the material properties as given by Gassmann (1951).

$$\frac{K_{\text{sat}}}{K_0 - K_{\text{sat}}} = \frac{K_{\text{dry}}}{K_0 - K_{\text{dry}}} + \frac{K_{\text{fl}}}{\phi(K_0 - K_{\text{fl}})}, \mu_{\text{sat}} = \mu_{\text{dry}}$$

where $\phi$ is the porosity, $\mu_{\text{dry}}$ and $K_{\text{dry}}$ are the dry framework shear and bulk moduli, respectively, $K_0$ is the mineral bulk modulus, $K_{\text{fl}}$ is the pore fluid bulk modulus, and $\mu_{\text{sat}}$ and $K_{\text{sat}}$ are the saturated effective bulk moduli, respectively.

For partially saturated rock at low frequencies, the effective modulus of the pore fluid is the harmonic average of the air bulk modulus $K_{\text{air}}$ and the water bulk modulus $K_{\text{water}}$ is

$$\frac{1}{K_{\mathrm{fl}}} = \frac{S_{\mathrm{w}}}{K_{\mathrm{water}}} + \frac{1 - S_{\mathrm{w}}}{K_{\mathrm{air}}}$$

where $S_{\mathrm{w}}$ is water saturation of the pore space. The density of the materials is

$$\rho = \phi[S_{\mathrm{w}}\rho_{\mathrm{water}} + (1 - S_{\mathrm{w}})\rho_{\mathrm{air}}] + (1 - \phi)\rho_{\mathrm{gr}}$$

where $\rho_{\mathrm{air}}$ and $\rho_{\mathrm{water}}$ are the gas and the liquid densities, respectively, and $\rho_{\mathrm{gr}}$ is the grain density. This is particularly interesting because in high porosity unconsolidated sand, the partially saturated sand has a lower velocity than the dry sand. Only at 100 percent saturation is the stiffness of the pore fluid high enough to increase the velocity (Bachrach and Nur 1998). These equations are of particular interest for this experiment because they are used to calculate seismic velocities from water saturations (Fig. 2.1). That data is then used to create a velocity model for use in the ray tracing algorithm.

## 2.2 Ray Tracing Theory

To compare the simulator results with the sand tank experiment, one must create a velocity model for the simulation data and use a ray tracing algorithm to predict the paths through the model (Fig. 2.3). Once the rays are traced, then a comparison of first arrival times is made to the first arrival times observed in the sand tank experiment. Because the ray tracing algorithm will be called hundreds or thousands of time in the course of modeling an experiment, it should be efficient, simple to use, and accurate. The ray tracing routine chosen is rayinvr developed by Zelt (1988).

The velocity model in rayinvr can be described as a series of trapezoidal blocks with vertical sides and upper and lower boundaries of arbitrary dip (Fig. 2.2). The compressional wave velocity $v_0$, at the point ($x_0$,$z_0$) within the trapezoid is given by

$$v_0 = \frac{[(v_1 m_2 - v_2 m_1)x_0 + (v_2 - v_1)z_0 + (v_1 b_2 - v_2 b_1)]}{[(m_2 - m_1)x_0 + (b_2 - b_1)]} \tag{2.1}$$

where $v_1$ and $v_2$ are upper and lower velocities within the trapezoid (Zelt and

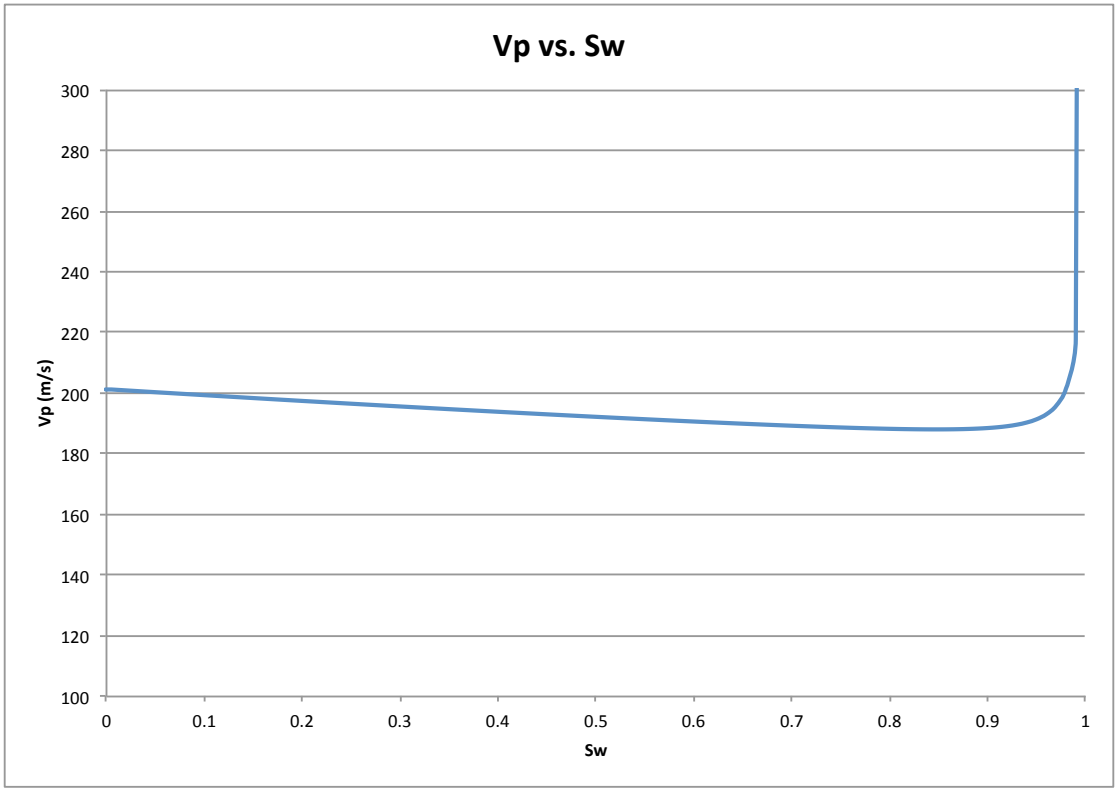


Figure 2.1: Water saturation vs. compressional wave velocity. Compressional wave velocity vs. water saturation in low velocity sand based on the Biot (1956b, Biot (1956a, Biot (1962) and Gassmann (1951) predictions. It is of interest to notice from 0-0.99 water saturation the velocity decreases and from 0.99-1 water saturation the velocity sharply increases. This is an interesting phenomena which will be discussed in detail throughout this thesis. This relationship between compressional wave velocity and water saturation is nonlinear.

Ellis 1988).

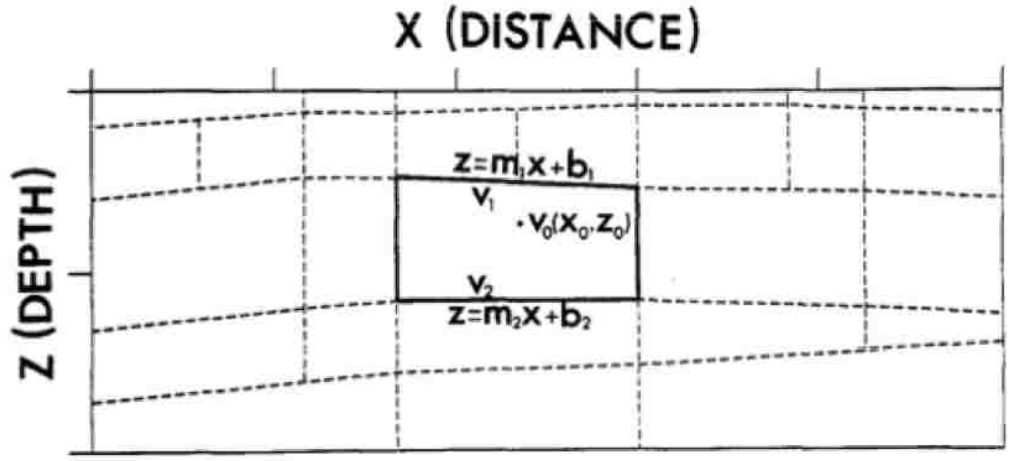


Figure 2.2: Rayinvr velocity model. An example velocity model consisting of five layers and twenty-seven trapezoidal blocks as shown by Zelt and Ellis (1988). Each trapezoid has vertical sides and upper and lower boundaries of arbitrary dip. Within each layer, the compressional wave velocity structure is defined by specifying a single upper and lower layer velocity for each line segment of the upper and lower layer boundary.

To trace rays through the velocity model, the ray tracing equations are solved numerically (Cerveny, Molotkov, and Psencik 1977; McMechan and Mooney 1980). The two-dimensional ray tracing equations solved by the routine are a pair of first order ordinary differential equations in two sets:

$$\frac{dz}{dx} = \cot\theta \tag{2.2}$$

$$\frac{d\theta}{dx} = \frac{v_z - v_x \cot\theta}{v} \tag{2.3}$$

and

$$\frac{dx}{dz} = \tan\theta \tag{2.4}$$

$$\frac{d\theta}{dz} = \frac{v_z \tan\theta - v_x}{v} \tag{2.5}$$

with initial conditions

$$x = x_0, z = z_0, \theta = \theta_0$$

where $(x_0, z_0)$ is the source location and $\theta_0$ is the ray take off angle (Cerveny, Molotkov, and Psencik 1977). The variable $\theta$ is the angle between the tangent to the ray and the $z$ axis, $v$ is the velocity, and $v_x$ and $v_z$ are partial derivitives of velocity with respect to $x$ and $z$ (Zelt and Ellis 1988). To solve either system, the routine uses the Runge Kutta method (Sheriff and Geldart 1983) with error control suggested by Cerveny, Molotkov, and Psencik (1977). To complete the ray tracing algorithm, Snell's law must be satisfied at each point of intersection of a ray with a model boundary (Zelt and Ellis 1988).

The ray step length $\Delta$ used in solving (Eq. 2.2 - 2.5), an increment in either the $x$ or $z$ direction, is given by the relationship

$$\Delta = \frac{\alpha v}{|v_{\mathrm{x}}| + |v_{\mathrm{z}}|} \tag{2.6}$$

where $\alpha$ is a user specified constant. Since the velocity given by (Eq. 2.1) and its partial derivatives are analytic functions of position, (Eqs. 2.2 - 2.5) can, in conjunction with (Eq. 2.6), be solved efficiently (Zelt and Ellis 1988).

## 2.3 First Break Picking

In this experiment the first arrivals of the seismic observations are estimated for later comparison to the first arrival times from the simulation models. For this experiment a conventional method for picking first arrival times on our seismic data was used. The analysis was performed using free, easy–to–use software (Geogiga Technology Corp. 2012, Front End 7.1), which analyzes the trace amplitudes directly. Furthermore, the picks can be easily output as an ASCII file for later use, for example, in the inversion process.

A conventional, visual handpicking, method was used in this case for first break picking because there is a limited amount of seismic data collected experimentally (Fig. 2.4). In some cases a more robust method might be desirable for processing large amounts of data, but in this experiment it is not needed. Other methods

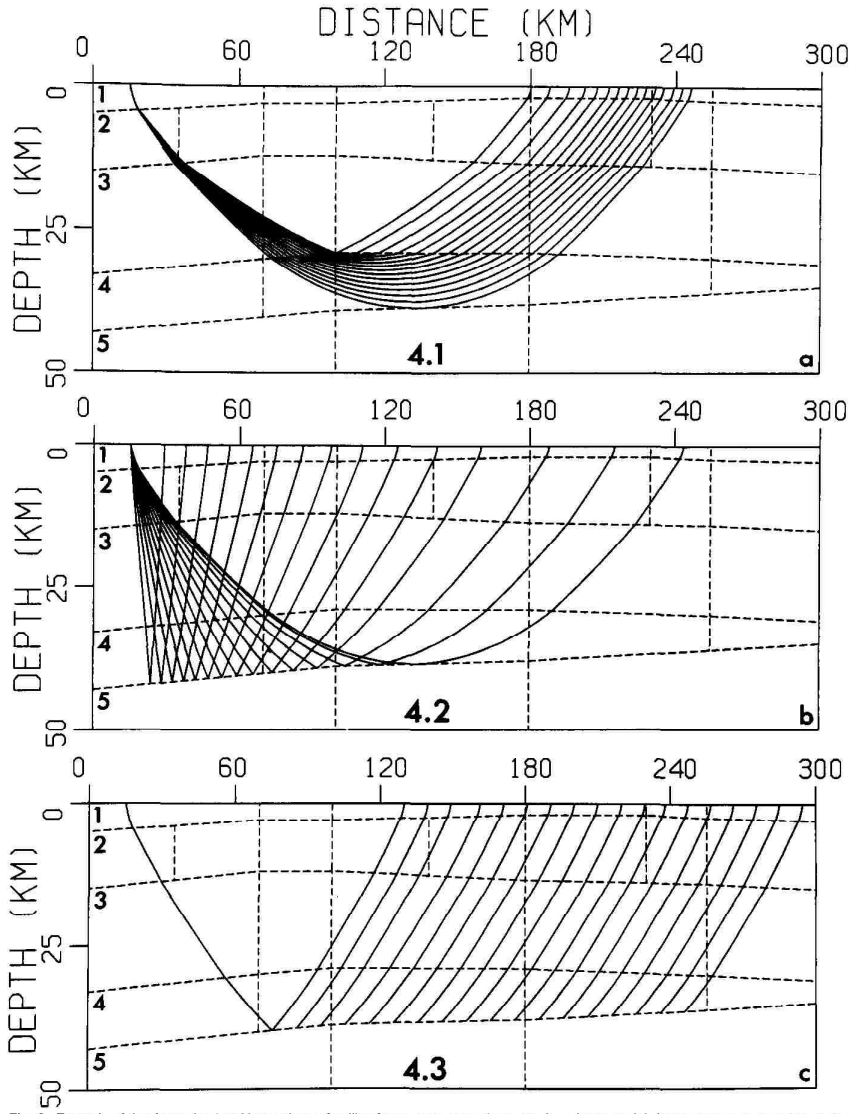


Figure 2.3: The three ray families. Example of the three simplest kinematic ray families for a single layer of a five layer model. Turning rays (a), reflected rays (b), and critical refraction (head waves) (c) as described by Zelt and Ellis (1988). The horizontal cross-sections labeled one through five represent different layers in the velocity model. It is important to notice the refracted wave paths in (a) because it is these refractions that will be used to provide first arrival times in this experiment.

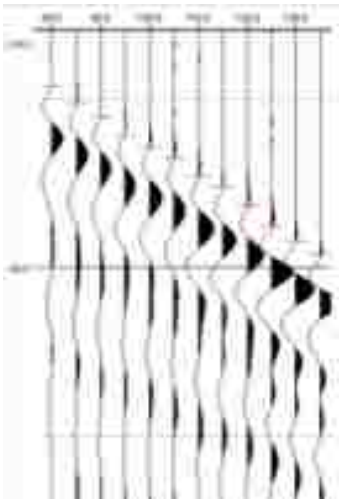

Figure 2.4: First break picking. Picking first breaks in seismic data Geogiga Technology Corp. (2012). Notice the first break is represented as the first considerable change in the amplitude of each trace in the survey. The first break picks from the observations are compared with the calculated first arrival times from the velocity model derived from the flow model, and calculated in rayinvr.

for reducing noise or emphasizing the first arrivals have yielded better results in some instances, but a robust method applicable to a variety of data types has proven difficult. Control algorithms that attempt to keep the picks from wandering have also been complicated and produced variable results (Criss, Kappius, and Cunningham 2003).

For comparison, an automatic first break picking algorithm in Seismic Unix (Stockwell and Cohen 2008) was tested against the conventionally picked first break times from the Geogiga software. For the purpose of this experiment it is assumed the handpicked times are accurate, the first break picking algorithm will be compared to those values on the assumption. Using the hand picked first arrivals as calibration, it was concluded that the auto-picking program from seismic unix was less accurate to a large degree. As shown in Figure 2.5, it is evident the auto-pickers fractional error is greater than 50 percent. If the first nine picks, the receivers that are closest to the source, are thrown out the fractional error decreases to less than 30 percent in wet sand and less than 10 percent in dry. It appears that for the nearest receivers, the first nine, the small distance from the source causes relatively high–amplitude surface waves that interfere with the auto-picking algorithm. The fractional error increases when water is present in the tank, perhaps because the saturated media causes an increased amplitude in the surface waves, again interfering with the auto-picking routine.

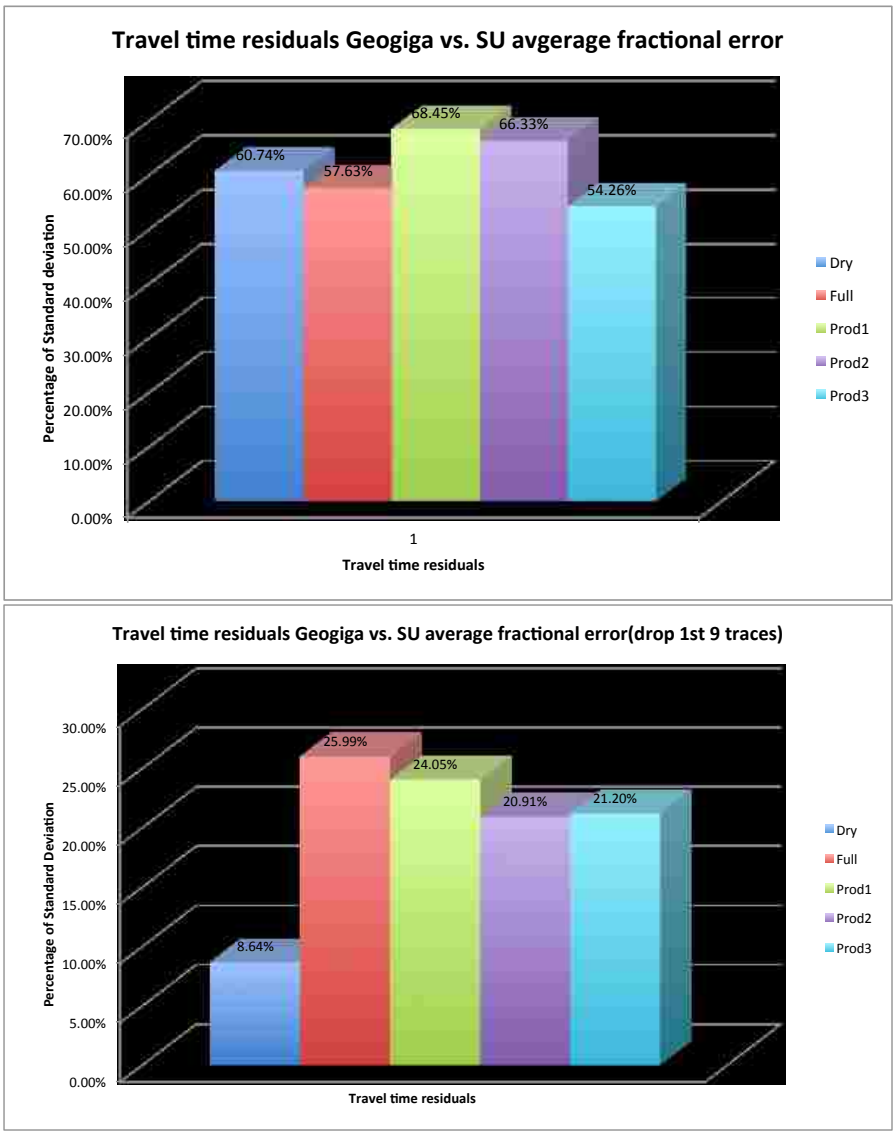


Figure 2.5: Travel time comparison handpicked vs. auto-picked. Shown above are the travel time comparisons for handpicked times vs. auto-picked times. The comparison is based on the assumption the handpicked first arrivals times are correct. When the first nine traces are thrown out the fractional error decreases dramatically. Also, when there is not water in the tank the fractional error is decreased even more. It is evident the auto-pickers fractional error decreases by 50 percent if the first nine picks (the receivers that are closest to the source) are thrown out. The fractional error decreases to less than 10 percent when the first nine picks are thrown out and the sand tank is empty.

## 2.4 Flow Equations

In the mid 1800's a French engineer named Henry Darcy made the for systematic study of the movement of water through a porous medium(Darcy 1856). Darcy found that the flow in a pipe will be proportional to the cross-sectional area of the pipe. Combined with a proportionality constant, K, also referred to as hydraulic conductivity; the expression became known as Darcy's Law (Fetter 2001).

$$Q = -KA\frac{dh}{dl}$$

Where $k$ equals the intrinsic permeability multiplied by the density and acceleration due to gravity all divided by the viscosity of the fluid.

$$K = k\frac{\rho g}{\mu}$$

Using Dupuit assumptions Bear (1979) provides an equation to describe radial flow to a well in an aquifer where H and h are the heads at the outer and inner boundaries and $R$ and $r$ are the radii at the outer boundary and the well (Fig. 2.6). The Dupuit assumptions state that groundwater moves horizontally in an unconfined aquifer and that the groundwater discharge is proportional to the saturated aquifer thickness. It also requires that the water table is relatively flat and is hydrostatic (Dupuit 1863).

$$Q_w = \pi k\frac{\rho g}{\mu}\frac{H_0^2 - h_w^2}{ln\frac{R}{r_w}}$$

Then finally

$$q = \frac{2\pi kh}{\mu B}\frac{H_0^2 - h_w^2}{ln\frac{R}{r_w}}$$

This equation is also one of the base equations used when Johns et al. (2005) explores the prediction of capillary fluid interfaces during gas or water coning in vertical wells. This coning idea and equation is important in the sand tank

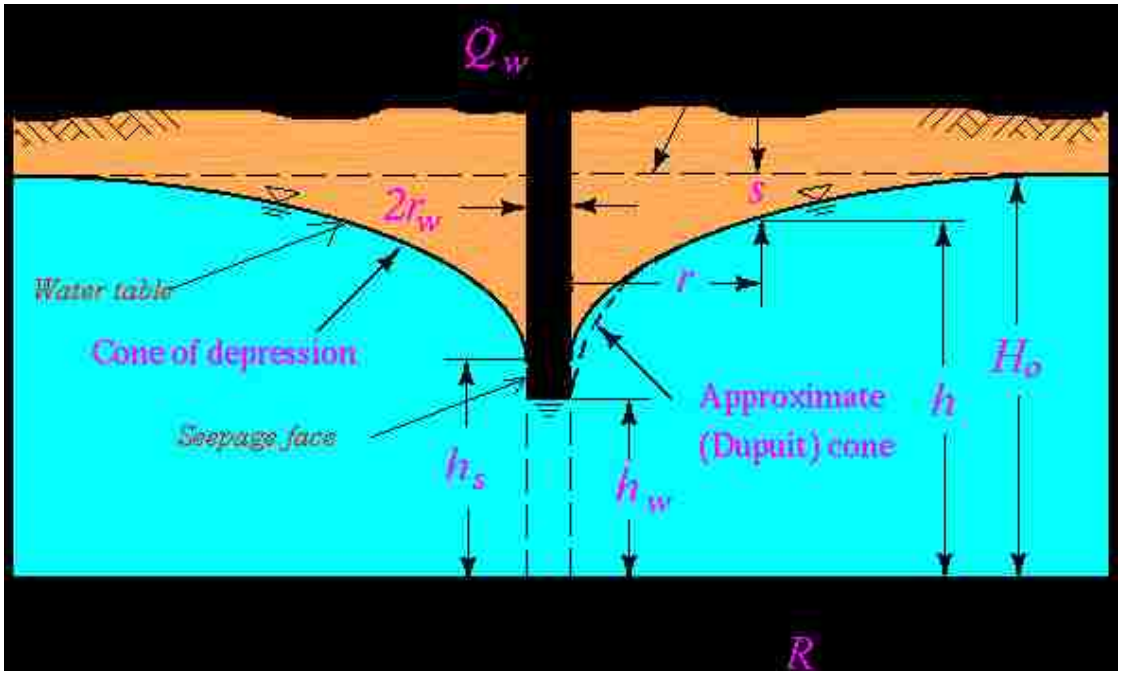


Figure 2.6: Radial flow to a well as described by Bear (1979). This idea will illustrate the flow patterns in the sand tank experiment. The Dupuit assumptions state that groundwater moves horizontally in an unconfined aquifer and that the groundwater discharge is proportional to the saturated aquifer thickness. It also requires that the water table is relatively flat and is hydrostatic (Dupuit 1863).

experiment because this helps to explain and predict flow behavior while acquiring production data as shown later in this thesis.

## 2.5 Seismic Resolution

Seismology is a widely–used subsurface geophysical imaging method because of its large range of penetration depths, from less than a meter to hundreds of kilometers (Bachrach and Nur 1998). In reflection it is desirable to enhance the high frequency component of the seismic signal and to remove lower frequency noise; this improves resolution of finer–scaled structures (Burger, Sheehan, and Jones 1992).

First, let us define a wavelength $\lambda$ (m) as a spacial period of wave that is calculated by

$$\lambda = \frac{v}{f}$$

Where $v$ is the velocity (m/s) and $f$ is the frequency (Hz). Many seismologists maintain that the limit of vertical resolution is $\lambda/4$ (Sheriff and Geldart 1983). However, for surveys less than 200 m deep, the more likely limit is $\lambda/2$ (Burger, Sheehan, and Jones 1992). That is how frequency affects vertical resolution, but frequency also affects horizontal resolution. Better horizontal resolution is achieved with higher frequencies just as with vertical resolution (Burger, Sheehan, and Jones 1992). Geophone spacing is also important in determining the detail of the sampled subsurface. For horizontal reflecting surfaces, the area of reflection is located about halfway between receiver and source (Burger, Sheehan, and Jones 1992). For instance if we have a geophone spacing of 2 m, we are sampling the subsurface at intervals of 1 m.

Seismic compressional wave velocities expected in unconsolidated, unconfined sand are on the order of 100 m/s (Bachrach and Nur 1998). If the dominant or maximum frequency acquired is 5 kHz, the wavelength (m) in the sand tank is

$$\frac{100}{5000} = 0.02$$

and using the relationship $\lambda/2$

$$\frac{0.02}{2} = 0.01$$

the resolution in the sand tank is approximately 1 cm.

## 2.6 Frequency Scaling of Geomodel

Because seismology can be used to image features on multiple scales, it lends itself to the modeling for this work. There are, however, several important considerations. Seismic physical modeling has assumptions and limitations, such as scaling, that need to be addressed (Smolkin 2011).

As previously stated, seismic compressional wave velocities expected in unconsolidated, unconfined sand are on the order of 100 m/s (Bachrach and Nur 1998). The dominant or maximum frequency acquired is 5 kHz and the wavelength is 2 cm. Typical velocities in the field can vary a little but are generally around 2000 m/s and frequencies are near 100 Hz

$$\frac{2000}{100} = 20$$

for a wavelength of 20 m. The ratio of the two wavelengths

$$\frac{20}{0.02} = 1000$$

provides our scaling factor of 1000. Meaning 1 m in the wavetank can be scaled to about 1000 m in the field.

## 2.7 Limitations

There are limitations to the data that can be collected in any experiment. For our experiment we chose to use the wave tank in the Geology Building, we call it the sand tank experiment. Here is a list of some of those limitations.

1. The easiest geologic medium to use in a lab experiment is sand. The sand is unconsolidated and relatively homogenous. The grain size of the sand within the tank is ca. 300 microns as per analysis by Smolkin (2011, Fig. 2.7 in this thesis). This will limit our physical experimental model to porosities and permeabilities of approximately 0.35 and 60 Darcys respectively. In the case only one was known the other could be found by the Carman-Kozeny relationship (Carman 1937).

2. Because of the large volumes of liquid in the sandtank experiment, water, as opposed to oil, is the preferred liquid. Water is safe, inexpensive, easy to clean up, has virtually constant values such as viscosity and compressibility at the conditions in the sand tank, and is well documented in its behavior in unconsolidated sands.

3. The reservoir (sand tank) is bounded and those boundaries cannot be changed. Even though the shape of the actual sand in the tank can be manipulated, the boundary conditions will remain constant. There is also an open pool in one end of the tank which provides constant fluid supply to our sand reservoir.

## 2.8 Key Points

- Seismic p (compressional) and s (shear) wave velocities can be used to find water saturation with the use of the Biot-Gassman equations.
- Ray tracing algorithms can be used to estimate first arrival times of synthetic velocity model.
- First arrival times of experimentally collected seismic data can be compared to calculated first arrival times from synthetic velocity models and residuals to be computed.
- Seismic resolution in the sand tank is ca. 1 cm.
- The scaling factor for seismic response is 1 m in the tank $\cong$ 1000 m in the field.

| Upper sand | Mean (phi) | Sorting | Skewness | Kurtosis |
|---|---|---|---|---|
| Sample 1 | 1.39809 | 0.47276 | 0.02907 | 0.87441 |
| Sample 2 | 1.19215 | 0.38624 | 0.19763 | 1.02865 |
| Sample 3 | 1.55965 | 0.47308 | -0.20508 | 0.9656 |

| Lower Sand | Mean (phi) | Sorting | Skewness | Kurtosis |
|---|---|---|---|---|
| Sample 4 | 1.71525 | 0.4334 | -0.02354 | 1.02947 |
| Sample 5 | 1.71308 | 0.43739 | -0.0172 | 1.03231 |
| Sample 6 | 1.69172 | 0.47574 | -0.02544 | 1.06852 |

| Diameter (mm) | Diameter (phi) | Wentworth Size Class | |
|---|---|---|---|
| 4096 | -12 | | Boulder |
| 256 | -8 | Gravel | Cobble |
| 64 | -6 | | Pebble |
| 4 | -2 | | Granule |
| 2 | -1 | | Very Coarse Sand |
| 1 | 0 | | Coarse Sand |
| 0.5 | 1 | Sand | Medium Sand |
| 0.25 | 2 | | Fine Sand |
| 0.125 | 3 | | Very Fine Sand |
| 0.0625 | 4 | | Coarse Silt |
| 0.0313 | 5 | | Medium Silt |
| 0.0156 | 6 | Silt | Fine Silt |
| 0.0078 | 7 | | Very Fine Silt |
| 0.0039 | 8 | | Clay |
| 0.00006 | 14 | Mud | |

Figure 2.7: Grain size within the sand tank. Above: Analysis of grain size within the sand tank performed by Smolkin (2011). Below: Particle size chart as presented by Wentworth (1922). The grain size of the sand within the sand tank is a medium grain sand, on the order of 300 microns.

# Chapter 3

# Objectives

## 3.1 Hypotheses

The hypothesis of this study is flow models are an adequate way of predicting flow in the sand tank.

## 3.2 Anticipated Results

The main objective of this experiment is to observe fluid flow through an unconsolidated sand reservoir and collect pressure, fluid flow rate, and seismic data. The observed data will then be compared to flow model data produced from simulations. There will be some major challenges to produce accurate flow model data relative to the observations from the sand tank experimental data. There is a high possibility that the observation data will have several complications involved in the interpretation process. Things like capillary forces, viscous pressure drop due to fluid flow, and seismic wavelengths, will make the observed data more unpredictable. The sensitivity of the first arrival times of the seismic survey due to the variation of saturation distribution in unconsolidated sand will be virtually impossible to predict. It is likely that the observed data will not match the predicted flow model data with any measure of accuracy. Some specific challenges matching experimentally observed data to the flow model data are listed below.

- The primary challenge is the action of the capillary forces in the sand tank.

The sand reservoir holds water in weeks after drainage and also holds air in days after be filled with water (there is little time to let the water infiltrate the formation, seven hours on average, and not much longer as the tank has a leakage problem). This variation of saturation in the sand tank wreaks havoc on the seismic surveys. Seismic velocity is affected by saturation (Bachrach and Nur 1998) and the objective of the observation data matching to simulated data is to verify the integrity of the synthetic model. If the seismic data is inconclusive it is less useful. In short, the capillary forces at work in the sand tank will not allow a clear seismic image of where 100 percent saturation starts and where the capillary fringe begins (Smolkin 2011). Bear illustrates this point in the image below (Fig. 3.1).

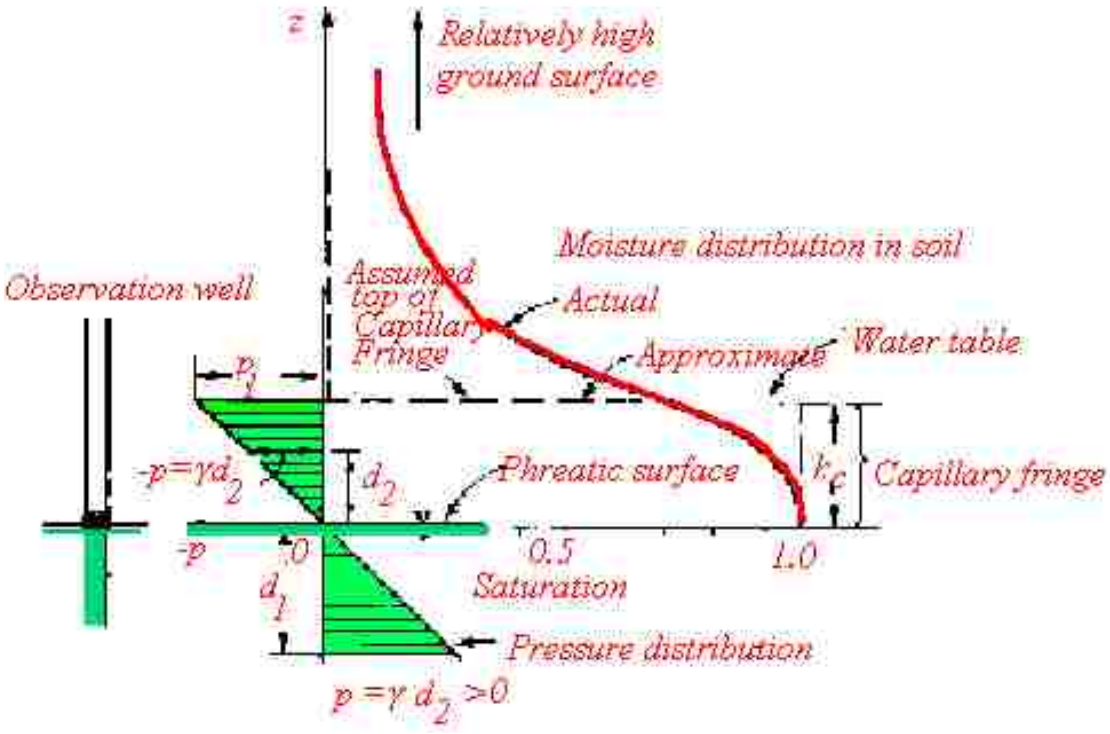


Figure 3.1: Capillary forces at work illustrated by Bear (Bear 1979). As shown, water saturation increases with depth (pressure), however, in the sand tank there is no point at which the sand pack becomes one hundred percent saturated with water. That makes it difficult to predict the precise fluid level in the tank. The whole sand tank is only partially saturated and behaves as such. It is difficult to identify any capillary fringe or zero tension surface.

- Another challenge is to work within the boundaries of our water supplied due to viscous pressure drop to fluid flow through the sand and also through the production well. As illustrated later in this thesis, there is a certain amount of skin caused not only by the sand buy by the production well itself. The exact

production rates and perforation sizes must be achieved to create maximum results. Producing the well too fast will result in rendering the well dry and producing too slow will show hardly any effect in the reservoir. Predicted flow rates are illustrated in graph below (Fig. 3.2).

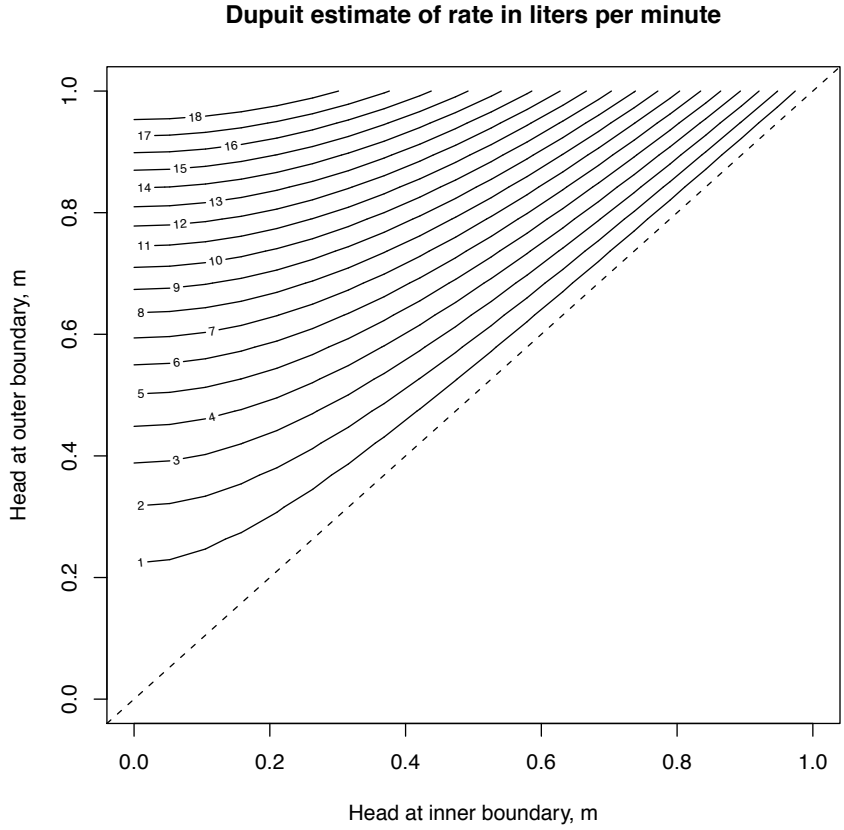


Figure 3.2: Sand tank flow rates using the Dupuit Approximation. Flow rates for various heads using the Dupuit approximation per White (2011) as presented by Bear (1979). Capillary pressure and relative permeability are neglected, dimensions and properties are appropriate for the sand tank experiment. For the projected heads at the inner at outer boundary a flow rate of approximately 1 liter per minute (.25 gallons per minute) is expected.

## 3.3 Key Points

- Hypotheses is that flow models are an adequate way of predicting fluid flow in the sand tank.
- Challenges such as capillary forces will make predicting water saturation with seismic velocities difficult.

# Chapter 4

# Methods

The methods used for the sand tank experiment are discussed in this chapter. Each major component is listed in section.

## 4.1 Workflow

The sand tank experiment consists of collecting both experimental seismic and production data and processing of the same. This also includes first break picking of sampled arrival times and running the ray tracing routine on the velocity model from the simulation data. The tasks that must be performed in the sand tank project from start to finish are described in more detail in this flow chart (Fig. 4.1).

1. Get the sand tank ready for experimentation. This includes construction and setup of all software and hardware needed for data collection as well as calibration of the same. Making sure that everything is functional and the experiments are carried out using the same protocol from one run to the next.

2. Collect and process all observed data from experiment, both production as well as seismic. This includes all pressure and flow meter data as well as seismic arrival data. This will also include locations of all monitoring wells, and sensors in each well as they change from run to run. Also included here will be the locations of the accelerometers as well as the location of each shot taken in an experimental run.

3. Pick first arrival times of collected seismic data. For reasons explained in chapter one, the first break picking is done in the conventional manner as opposed to using an automatic picking algorithm.

4. Perform ray tracing routine on information provided from simulation process. This information will include velocity model information as well as location information for all sources and accelerometers.

5. Analyze results. This includes comparing experimentally collected first arrival time data to calculated first arrival time data, verification of experimental parameters, analysis of production data, and verification of results. Comparisons of experiment from one run to the next are also of interest when parameters are changed from run to run.

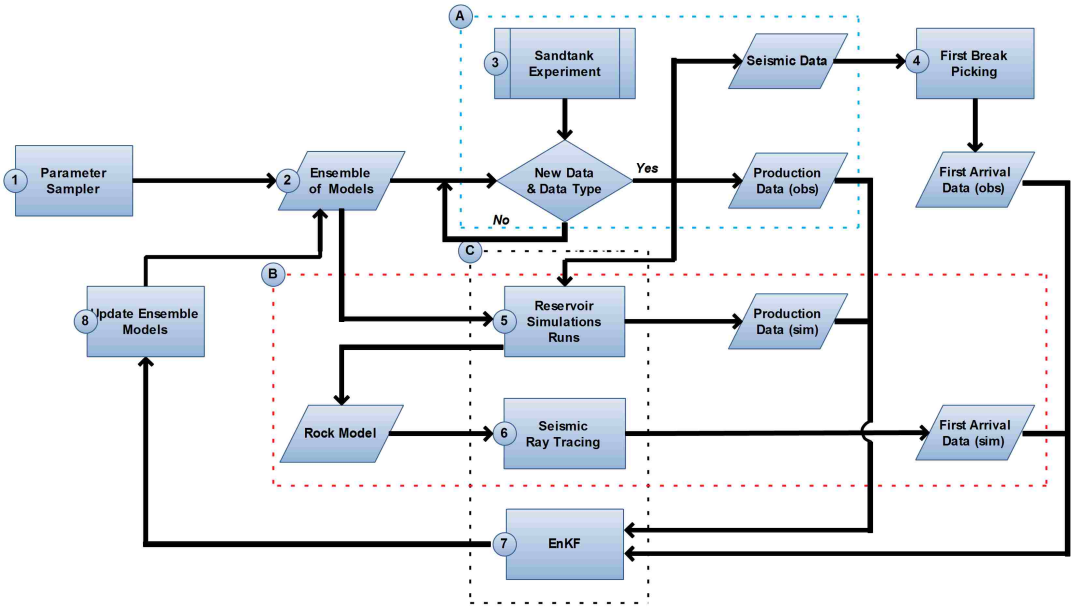


Figure 4.1: Workflow verification through the sand tank. Flowchart describing the individual tasks associated with the sand tank project. This is a multifaceted project with many groups working in unison, all facets are pictured here. There are contributions from the Petroleum, Geology, and Computer Science Departments respectively. The complexity of the tasks involved in this experiment make it a collaboration between multiple disciplines.

## 4.2 Equipment and Instrument Configuration

The sand tank experiment consists of multiple pieces of equipment running together in unison. Several extensive hardware and software packages have been installed

to both create and collect data.

### 4.2.1 Seismic Acquisition System

A unique seismic acquisition system was built by David Smolkin, former MS student of Dr. Juan Lorenzo (Smolkin 2011). A schematic of the seismic acquisition system is shown below (Fig. 4.2). The heart of the seismic data collection system is a National Instruments NI-PCI 6251 digital acquisition card. This DAQ card controls both signals for input (the signals coming from the accelerometers) as well as output (the signals going out from the source). The seismic source is an Etrema CU-18 ultrasonic transducer with a steel bolt installed in the end to help transfer the vibrations to the sand. This transducer can produce vibrations up to 20 kHz from DC voltage. The transducer is driven by a QSC Audio RMX 2450 audio amplifier set at a gain of about 24 dB. The geo-phones for this setup are ACH-01 accelerometer sensors manufactured by Measurement Specialties Inc.. The accelerometers are very sensitive to environmental noise and are shielded by copper tape adhered to the outside of each sensor (Smolkin 2011). To help complete the set up, Linear Technologies LT1115 operational amplifiers are used to further amplify the accelerometer's signals. Finally, the signals pass through a Behringer DI800 audio amplifier or DI Box before it returns to the DAQ card. For more detailed information on the seismic data acquisition system reference David Smolkin's MS Thesis (Smolkin 2011).

### 4.2.2 Production Data Acquisition System

Along with seismic observations in this experiment, production observations will also be made. The kinds of production data being collected are:

1. Pressure readings inside the production well, 4 monitoring wells, and the standing water at the free water end of the sand tank.
2. Flow rates being pumped form the production well.
3. Temperature readings from inside the production and monitoring wells are also possible but not needed in this experiment.

The data acquisition system for production data is similar to the seismic data acquisition system. The main component is the data acquisition card made by

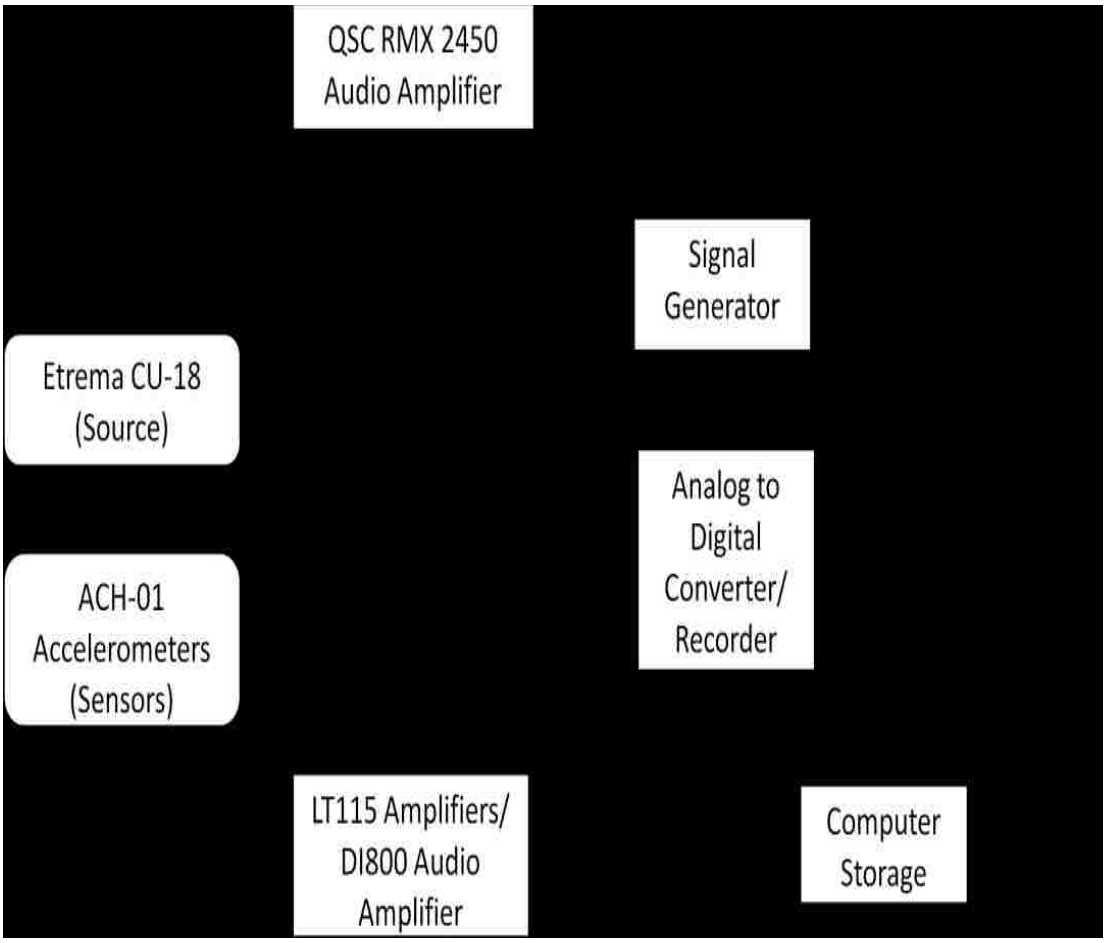


Figure 4.2: Seismic acquisition equipment schematic. Seismic Collection Schematic associated with the sand tank project. A National Instruments NI-PCI-6251 digital acquisition card (DAQ) serves as the core of the acquisition system, controlling the data input and output. It has high input and output rates and is able to record on 16 single-ended, or 8 differential, channels at a combined rate of 1 MHz (Smolkin 2011).

IOTECH. It is a DaqBoard/3000 Series PCI 16-Bit, 1-MHz Multifunction Board that is installed in a computer in the lab and run on a windows platform. The DaqBoard/3000 series has a 16-bit, 1-MHz A/D coupled with 16 single-ended, or 8 differential analog inputs. Seven software programmable ranges provide inputs from 10V to 100 mV full scale. Each channel can be software-configured for a different range, as well as for single-ended or differential bipolar input (Iotech Inc. 2005).

Connected to the DAQ card through a 68-pin SCSI connector are the WL400 Water Level Sensors, made by Global Water, which are calibrated to record pressures from 0-3 feet and temperatures from 0 to 50 degrees Celsius. These water level sensors produce an output of 4-20 mA which have to be connected to 250 Ohm resistors to drop the voltage between 0-10 V DC for pressure readings and 0-5 V DC for temperature readings. The sensors can be powered using a power supply of 10-36 V DC. For this experimentation a 12 V power source was chosen to power the sensors. The sensors are rated accurate to $\pm$ 1 percent of FS at constant temperature, 0.03 ft and 0.013 psi FS or 0.01 ft and 0.004 psi at a water depth of 1ft (Global Water Instrumentation, Inc. 2006).

Also connected to the DAQ card through the 68-pin SCSI connector is the FreeFlow P-Type Flow Transmitter. This flow monitor is made by Lake Monitors and can accurately measure flow in the 5-15 gpm range. The Measuring accuracy is rated $\pm$ 2 percent of FS (0.30 gpm FS or 0.005 gpm at 0.25 gpm) and repeatable at $\pm$ 5 percent of FS (Lake Monitors 2007). The flow monitor is attached by nylon hose in between the pump and the open end of the sand tank.

A 20 gpm-rated pump (Critical Velocity, LLC 2010) is used to produce water from the sand tank. To operate the pump at the low pumping rate needed for the sand tank it was necessary to install a 15 Amp Digital PWM Motor Speed controller (Critical Velocity, LLC 2010). The input voltage can be anywhere from 5.5 to 36 V DC and the potentiometer allows precision output voltage control to regulate the pumping speed. As with everything else a 12 V DC power source was used to power the speed controller, that in turn, powered the pump.

### 4.2.3 The Sand Tank

Lastly, is the physical reservoir model, the sand tank. The sand tank is the wave tank in the Geology Building at Louisiana State University. It is approximately $6 \times 9 \times 0.6$ m. The sand forms a reservoir formation which is 6 m in length on the bottom and 2 m in length on the top, forming a wedge. It extends the full width of the 6 m sand tank and is filled 0.5 m deep with sand. The sand is mixed with

slightly different sands and is believed to be relatively homogenous. There are five monitoring wells in the sand tank, four for observation and one for both production and observation. The wells are made from 2" (0.051 m) diameter PVC pipe that is machine slotted over the whole well at 10 slot, 0.000254 m slits. The sand tank with all experimental equipment set up and ready to collect data is pictured below (Fig. 4.3).

Figure 4.3: Sand tank data acquisition setup. The figure shows all five monitoring wells with PT sensors and all seismic data collection equipment ready to collect data. This is the equipment configuration used to collect observations for this thesis. Also, notice the capillary forces absorbing water up into the formation above the water line at the free water end of the tank.

## 4.3 Implementation

Using the aforementioned equipment and the sand tank, both seismic and production observations are collected and compared against the flow model simulation data. The data collection process starts in this fashion:

1. Fill the sand tank with water. This process is the most time consuming process in the collection of data.

(a) The tank is filled by a sump pump and a water reservoir which is small in comparison to the volume of the sand tank. The pump will pump the reservoir dry several times and will need to be cycled off when there is no water present to be pumped. The reservoir has to be pumped and filled several times before the sand tank reaches full experimental capacity of 12 inches or so of water at the open water end of the tank.

(b) After the process is complete, it is necessary to wait for approximately 7 hours before trying to collect data. This is done so the water has a chance to permeate throughout the entire sand formation.

2. While the sand tank is filling with water, both data collecting computers containing the DAQ cards should be started and the programs to collect the data should be engaged.

   (a) To collect the production data the IOTECH DAQ card has a factory made interface named Daqview with which to view, control, and collect data.

   (b) To collect seismic data the National Instruments DAQ card has a factory made interface named Loqview with which to view, control, and collect data. It should be noted that this is an excellent time to enter all of the collection parameters into the interface software if the parameters have changed since the last use or if a new session has been started.

3. Starting with the production data collection equipment first, set up all the equipment, making sure it is all working correctly.

   (a) The water level sensors should each be hooked up to their 12 V power source and tested in a 5 gallon bucket of water to make sure each one is working correctly.

   (b) Each monitoring well is numbered by location and each sensor is numbered with a location number. The sensors should be placed one in each well that corresponds to the correct number. There will be one extra sensor that should be placed in a location in the free end of the tank and the location in $x$ and $y$ coordinates should be entered into the location file.

   (c) Next, the Critical Velocity Speed Controller should be connected to a 12 V power source and the connected to the pump to make sure all is working correctly. If the pump is receiving power disconnect it and connect the flow meter to its 12 V power source.

   (d) After everything is connected to power and all is working well stick the pumping end of the hose into the 5 gallon bucket and begin to pump water out while calibrating the speed controller. During this process water must continually be added to the bucket to make sure it does't

run dry. Also, the pump may need to be primed to start the pumping process.

4. After all is working correctly above, set up the seismic data collecting equipment. The computer containing the DAQ card will have to be rolled over to the edge of the tank and all the amps and collection equipment should be placed neatly in order.

   (a) The 8 accelerometers acting as geo-phones should be carefully laid out and connected to the amplifier boxes and the power source. The accelerometers should then be places in the sand at equal spacing and measured locations from each other. The locations should then be entered into the location file in the production computer.

   (b) The source should be set out and placed in it's first shot location, this location should be measured as well as each subsequent shot location. This information should then be entered into the location file.

   (c) After all the seismic equipment is set up, collect some test data first to make sure all is working correctly. If it is all working correctly then proceed to the next step. Note: If data collection in an empty tank is warranted, then the seismic data collection equipment may be set up before the production equipment to take readings of a dry tank. But proceed the same way as the instructions go, only the order will be different.

5. The next phase is data collection.

   (a) Make sure there is power to all equipment.

   (b) Turn on the pump, which is still in the 5 gallon bucket.

   (c) Turn on the Daqview production data collection equipment set your time steps and data collection rate and start to collect data.

   (d) While the pump is still pumping quickly move the hose from the 5 gallon bucket into the production well.

   (e) Make sure that all the production equipment is collecting data properly and then move to the seismic equipment.

   (f) The power should already be connected. Start shooting seismic signals in the sequence is prescribed for the experiment.

6. After the seismic data collection is complete, turn off all the power to the equipment and remove it from the sand.

   (a) Next, turn the Daqview data collector off and power down all production equipment.

   (b) Let the water out of the tank and clean up the area, the data collection process is complete.

## 4.4 Data Formats

Data collection for the sand tank experiment will consists of a total of three different kinds of files. The first kind of file will be the seismic data files. These files are *seismic*(date).lvm format and contain approximately 6.2 MB of information. One such file will be present for each shot taken. There are eight geophones and a multiple of eight shots per shot line (this will work out best for the ray tracing algorithm to be used later), for a total of eight seismic files per experimental run. After the seismic observations are collected they will be processed using 3 separate scripts described in the Smolkin (2011) thesis. For more information on these scripts reference the Smolkin (2011) thesis. One script to stack the data, one to zero it out, and the final to shift the data to account for inaccuracies in accelerometer placement. The production data will be collected in binary file format but can be easily changed to ascii format with the software tools provided by the DAQ card. The name of this file is *production*(date).txt. This file will be less than 100 KB in most cases, and there will only be one per experimental run (unless otherwise warranted). The information contained in these files will be production well data, monitoring well data, and production flow rate. The last file will be the location file. It will have monitoring well locations, which will also be the locations of five of the six water level sensors, and source and receiver locations for the seismic data. This file is currently in excel format and there is only one. The name of this file is *Location*.xlsx. In the future it may be turned into 3 separate files and changed into a .csv format for system automation purposes. It should be noted the file must be hand created with user inputs, this file is not created by the production nor the seismic data collection equipment.

## 4.5 Challenges

Preliminary tests have unveiled several issues arising when attempting to run this experiment. As with every experiment there were some very unique and very relevant challenges to collecting data from the sand tank. During the last several months the complexities of data collection in the sand tank have revealed themselves. Some of these challenges have been documented below.

- The first challenge that needed to be addressed was sand control. How to keep sand out of the monitoring/production well so the pump will not get clogged. When initially pumping there was sand infiltrating the bottom, and possibly through the perforations, of the monitoring/production well because it wasn't enclosed. After placing a PVC cap on the bottom end

of the well pipe the sand problem was resolved. However, this introduced another problem, a skin type effect was encountered when pumping water through the PVC pipe even when not placed in the sand formation. A test was run placing the slotted PVC pipe in a 5 gallon bucket of water and placing the pump hose in the pipe and pumping water at several different rates while measuring the pressure inside and outside of the production well. The data is shown below (Fig. 4.4). As you can see from the data below, at about 6 GPM, the pipe was was causing a pressure drop in the production well equal to approximately 0.07 feet of water (0.030 psi). This provides evidence that without being in the formation, the water was losing approximately 0.84" of head, or 0.030 psi when being pumped at 6 GPM. Shown is a plot of pressure loss vs. flow rate using the calculated discharge coefficient for this experiment (Fig. 4.5). The formation cannot be pumped at this rate as proved by the Johns et al. (2005) representation of the Dupuit equation in chapter one. However, it does pose an interesting question: What is the skin factor being created by the slotted PVC pipe? This question with be examined in more depth in chapter four.

- Another challenge was determining the correct production rate to accommodate the skin effects of the pipe and the supply of the formation. So what is the optimal pumping rate? What size perforations are needed in the production pipe, how many, over what length? Slowing the pumping rate down to about .25 gpm seems to work well. This flow rate also is correct for the formation according the the Johns et al. (2005) representation of the Dupuit Equation when all the units are converted.

- Another challenge that is also related to production issues is the fact the flow meter is only quoted to be accurate between 5-15 gpm (Lake Monitors 2007). This is an issue because, as stated earlier, the formation and the PVC well pipe can only supply about 0.25 gpm. As a result the Daqview Data Collector has to be hand calibrated to measure such low flow rates.

- Another interesting issue experienced during experimentation is the capillary forces inside the sand formation have a tendency to soak up the water and saturate the entire formation and not just the formation up to the water level point. This creates a problem because of the sensitivity of the electronic equipment and components used in the seismic data collection part of the experiment.

- Lastly, is the sensitivity of the seismic data collection equipment. It needs to be handled with extreme care and great detail. This equipment had to be updated and upgraded several times during the duration of this experimental calibration period.

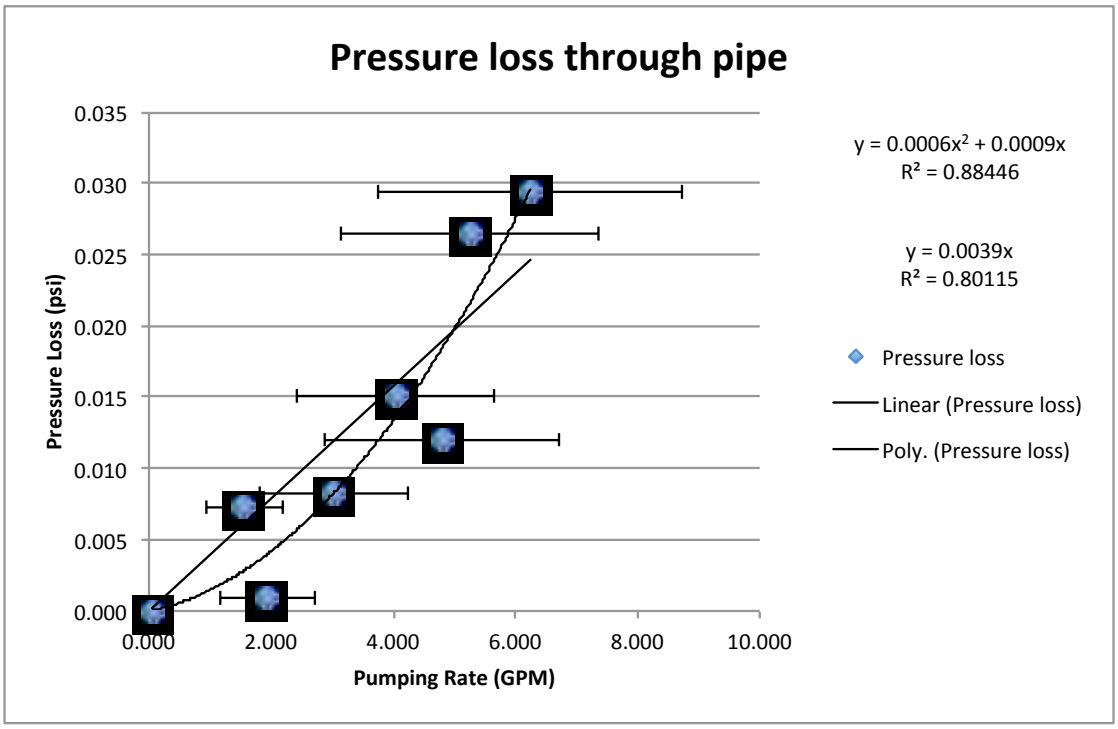


Figure 4.4: Preliminary pumping test through slotted PVC. A test was run placing the slotted PVC pipe in a 5 gallon bucket of water and placing the pump hose in the pipe and pumping water at several different rates while measuring the pressure inside and outside of the production well. Preliminary pumping test showing a pressure drop created by the slotted PVC. The water was losing about 0.07 feet of head (0.030 psi) when being pumped at 6 GPM. Of course the formation will need to be pumped at much lower rates, however, this pressure drop through the slotted PVC well pipe must be considered in the calibration of the overall experiment. The experimental observations of pressure loss vs. pumping rate can be fitted to both linear and polynomial slopes using an error margin, as discussed in more detail in chapter 6, though the accuracy of the polynomial fit is slightly better. For more detail on the flow in this experiment refer to Appendix D.

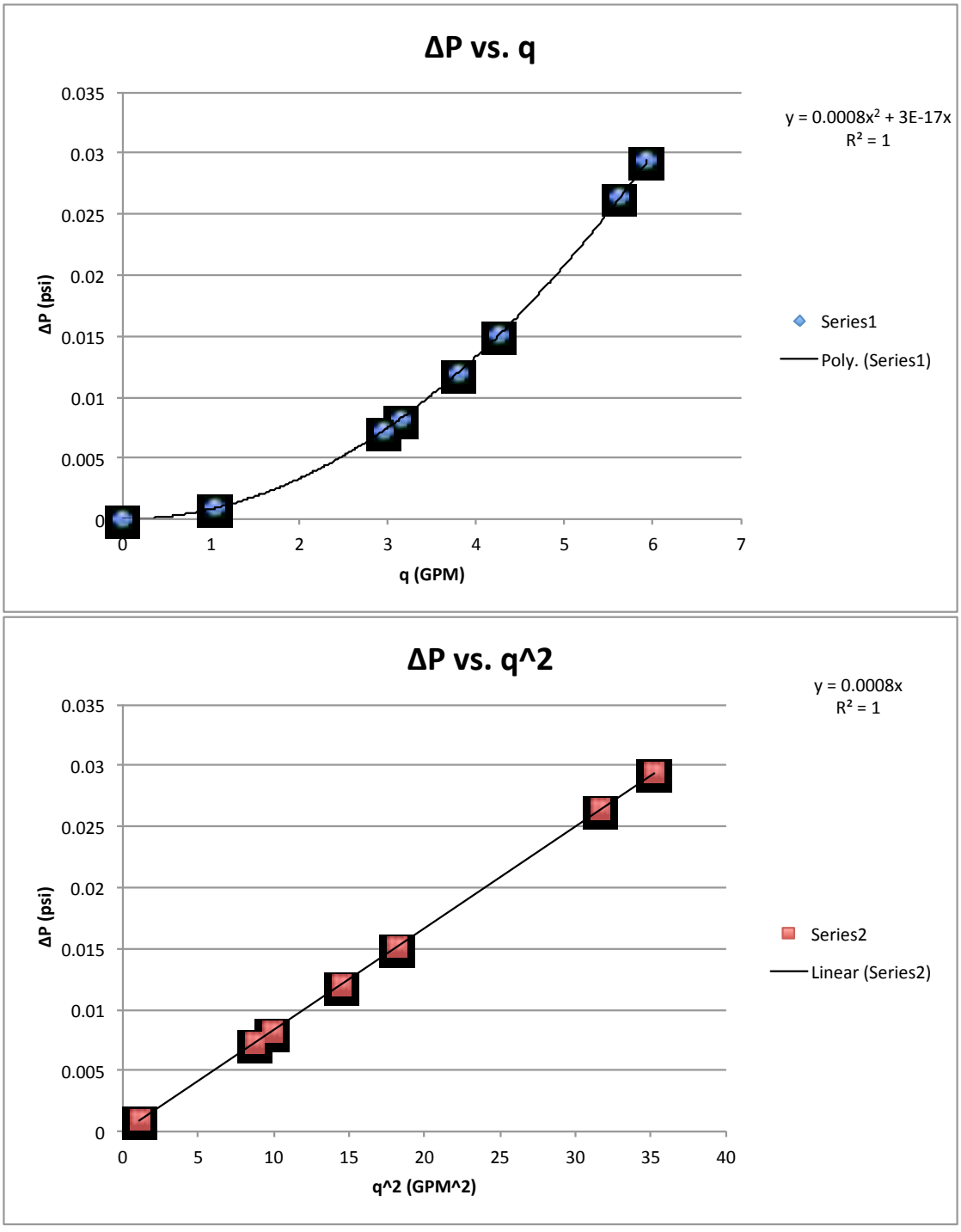


Figure 4.5: Pressure loss vs. flow rate. Above, using the calculated discharge coefficient (Appendix D) for this experiment, $C_d \simeq 1.2$, this plot represents the pressure loss vs. flow rate for our given pressure losses as presented earlier (Fig. 4.4). As shown the trend is a perfect polynomial fit which is expected for this calculation. Below, plotting the pressure loss vs. the square of the flow rate. The trend, as expected, is a straight line.

## 4.6 Key Points

- Task list for sand tank experiment:

    1. Collect and process all sand tank observation data.
    2. Pick first arrivals times of observed seismic data.
    3. Hand off observed production data to simulation team.
    4. Run ray tracing algorithm on seismic velocity model from simulation.
    5. Compare residuals with EnKF.

- This experimental setup includes both production and seismic data aquisition equipment.
- Data collection is performed in a carefully constructed sequence of steps.
- All data files and format are compatible with analysis software.
- Sand control, pressure loss through the PVC pipe, and flowmeter inaccuracy, all provide challenges for this experiment.

# Chapter 5

# Results

This chapter explains the calibration and testing of the experimental equipment in depth as well as complete results from running a full scale experiment as described in this thesis.

## 5.1 Calibration of Equipment

Prior to performing any of the experiments and accepting any of the results as they are, it is necessary to first calibrate all of the equipment used in experimentation. All of the equipment comes with factory calibration specifications however, as some of the calibration tests show, the factory specifications are not correct for this experimental setup.

### 5.1.1 Sand Tank Calibration

For this experiment, the initial part of the setup is the reservoir. The reservoir being used here is the afore mentioned sand tank. Pictured in Figure 5.1, are the locations of the experimental setup within the sand tank. One of the major challenges running this experiment is the time taken to conduct a full experimental run. Elementary tasks, such as filling up the sand tank with water are time consuming. As preliminary experimentation will show, it takes some time for the water to come to equilibrium when filling the tank as shown in Figure 5.2. It is important to know how long the water takes to reach equilibrium in the tank so

that the experiment is not run until water level equilibrium is achieved. This is important because it could skew the experimental results in a way not accounted for. Inversely, it also takes some time for water to completely drain from the tank when experimentation is over as shown in Figure 5.3. This is due to the capillary forces inside the sand pack. The capillary forces inside the the sand pack will hold residual saturation for several weeks, even months, after the tank has been drained. It should also be noted that the sand tank leaks a small amount of water out onto the floor, making it troublesome to run an experiment over several hours or days because it will flood the rooms in the Geology building adjacent to the tank.

### 5.1.2 PVC Production/Monitoring Well Calibration

There are five monitoring wells, the production well is also a monitoring well, located within the sand tank. A 2" circumslotted, ten slot (ten slots per inch) PVC pipe was used in the construction of the wells (Fig. 5.4). The slot size is 0.010", or 0.000254 m (Fig. 5.6). These slots act as perforations in the well bores of the sand tank. There is no production tubing inside the production wells, the well produces straight through the casing (Fig. 5.5).

Preliminary pumping tests show a distinct pressure drop even when producing through the slotted PVC only (Fig. 4.4). An experiment was conducted to calculate and quantify this *PVC skin effect*. For this experimental setup, the production well was placed in a five gallon bucket with a constant water source flowing (Fig. 5.7). While producing water from the well inside the bucket, the pressure inside and outside the well was recorded as well as the flow rate during the production period. The data was then analyzed and a skin factor was determined, in standard US units, from the following equation from (Horne 1995).

$$s = \frac{0.00708kh}{qB\mu} \triangle p_s$$

Where $s$ is the skin, $k$ is the permeability in mD, $h$ is the height in ft, $q$ is the flowrate in STB/D, $B$ in rb/STB, $\triangle p_s$ is the pressure difference in psi, and $\mu$ is the viscosity in cp. As defined, the skin factor is dimensionless and has no units. Using the slope from the graph of pressure drop vs. flow rate (Fig. 4.4), and the skin equation, a relationship was developed. The relationship is as follows:

$$\triangle p_s = \frac{141.2qB\mu}{kh} s$$

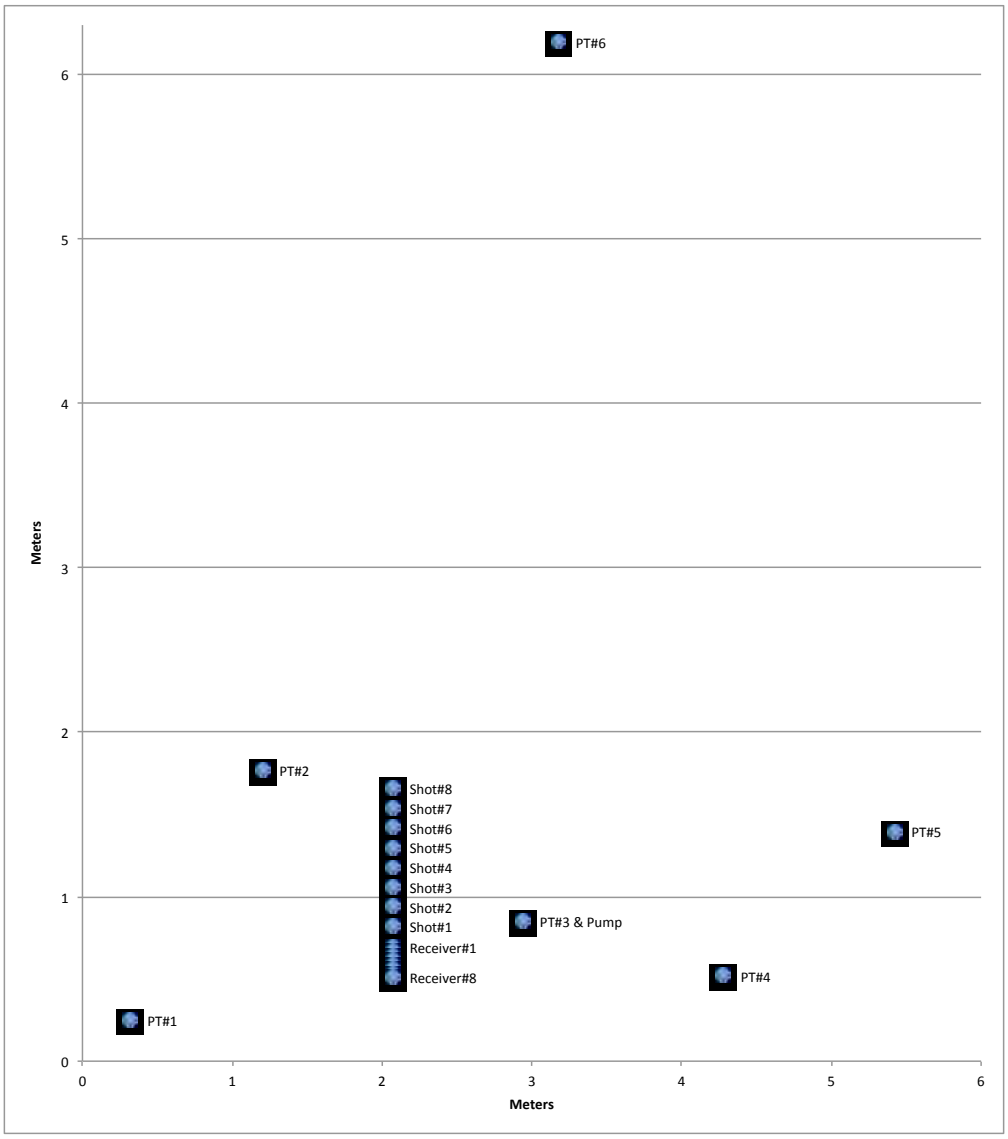


Figure 5.1: Seismic/Production data collection locations. Pictured above are all the pressure and temperature sensor locations and measurement information. Also shown are all source/receiver locations for the seismic data acquisition equipment. Receivers 2-7 are in between receivers 1 and 8 in the figure in order. They are not labeled because of legibility.

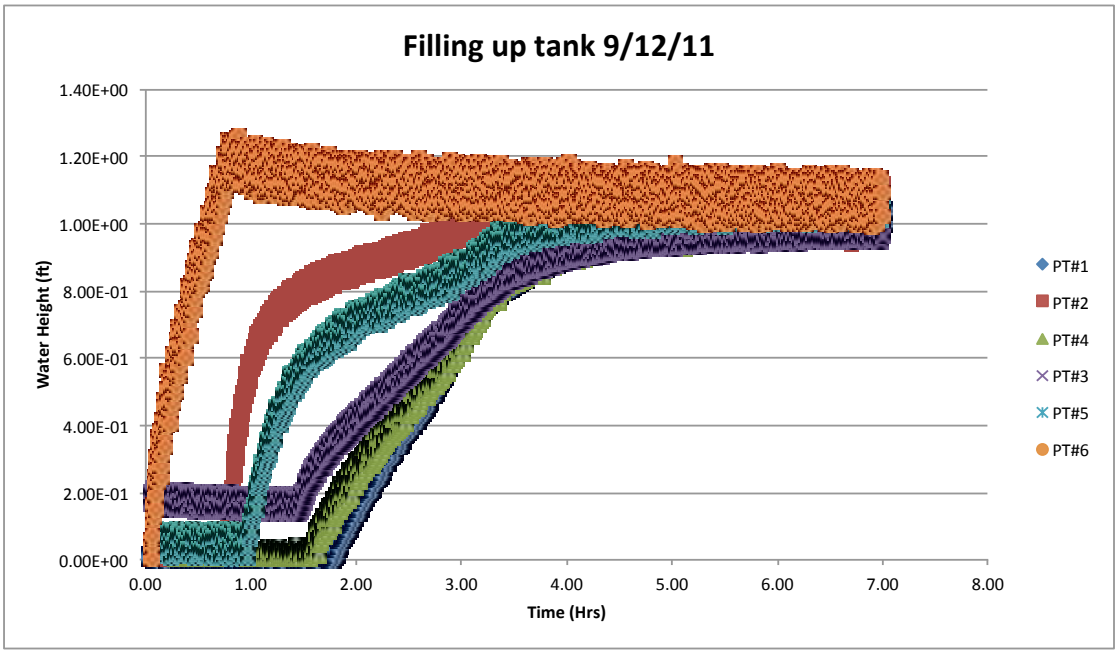


Figure 5.2: Time for water to come to equilibrium in tank. Illustrated above is the time it takes for water to come to equilibrium in the sand tank. The monitoring wells fill with water according to there locations relative to the open end of the tank. The water level in the open end of the tank fills relatively quickly and then levels off and lowers as water seeps into the formation.

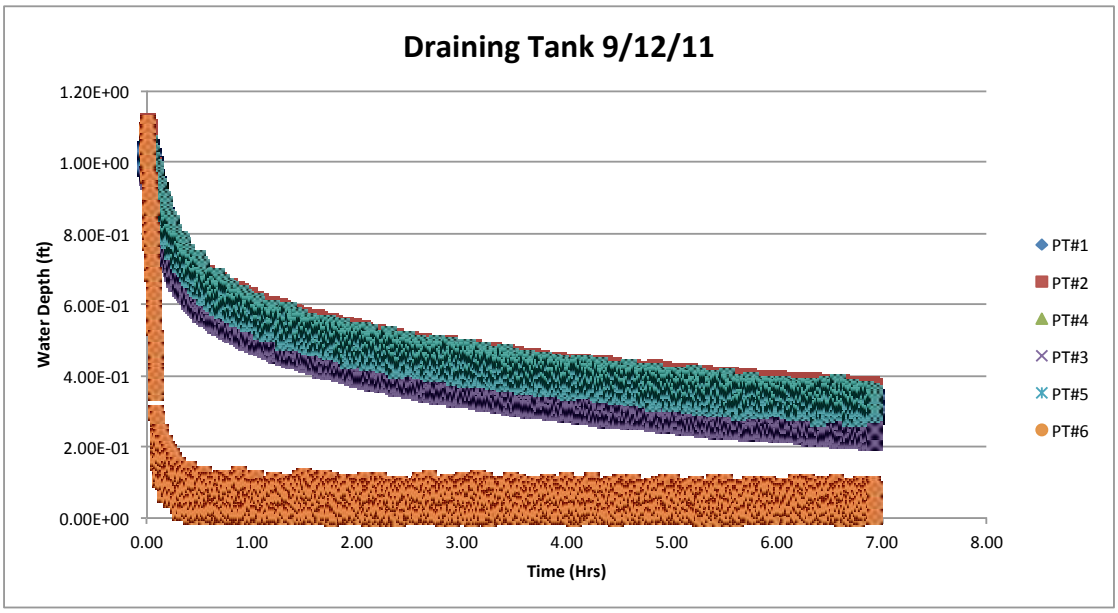


Figure 5.3: Time for water to drain out of tank. Illustrated above is the time it takes for water to drain from the sand tank. The wells do not deplete of water according to there locations relative to the open end of the tank. The water level in the open end of the tank depletes relatively quickly and then levels off. The monitoring wells drop off at a much slower rate as water seeps out of the formation.

$$\frac{\triangle p_s}{q} = \frac{141.2B\mu}{kh}s$$

$$0.0039 = \frac{141.2}{k}s$$

$$\frac{0.0039}{141.2} = \frac{s}{k}$$

$$0.000028 = \frac{s}{k}$$

in the sand tank k $\simeq$ 70 D, so the skin factor in the sand tank (Fig. 5.8) is

$$s \simeq 2$$


Figure 5.4: Slotted PVC used for wells in sand tank. Pictured above is the 2" circumslotted, ten slot (ten slots per inch), PVC pipe used in the construction of the wells within the sand tank. The slot size is 0.010", or 0.000254 m. These slots act as perforations in the well bores of the sand tank. There is no production tubing inside the production wells, the well produces straight through the casing.

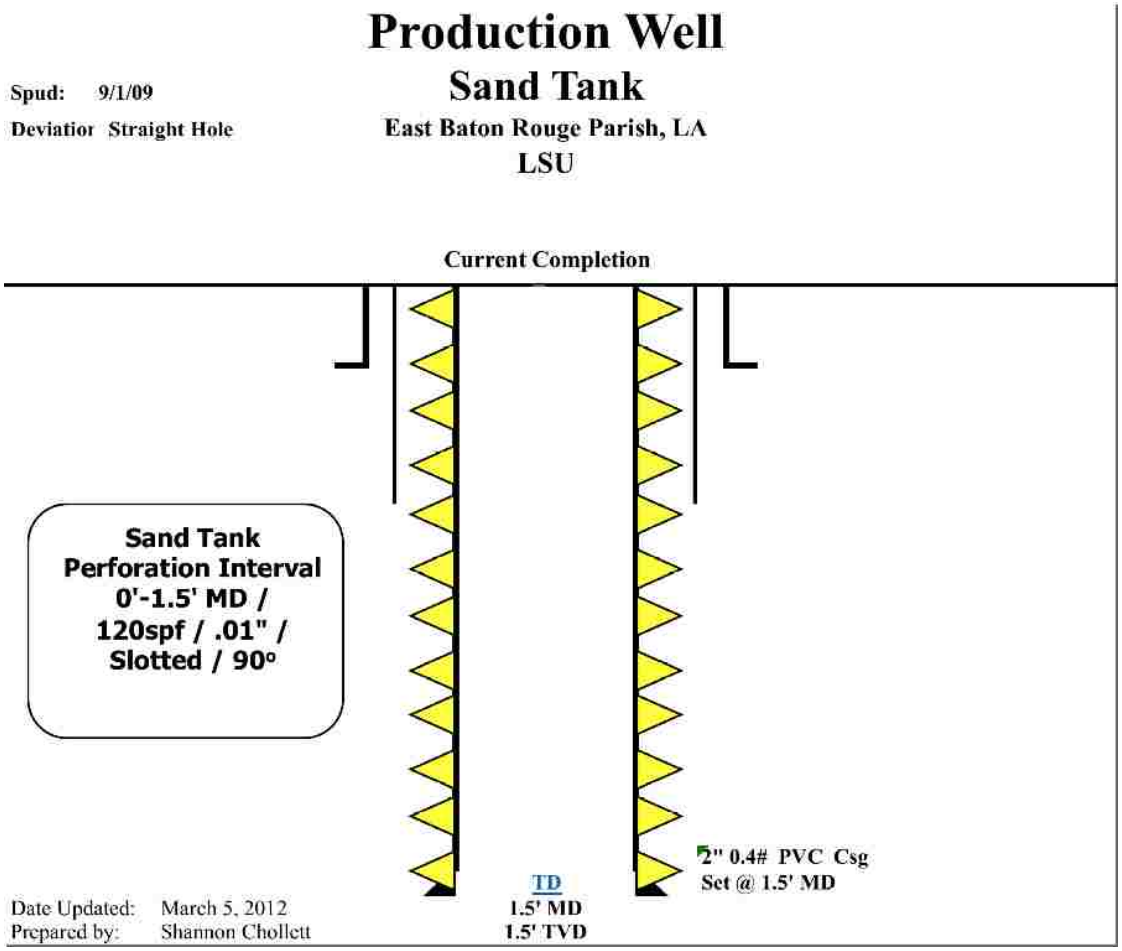


Figure 5.5: Wellbore Schematic. Pictured above is the wellbore schematic of the wells within the sand tank. The well is perforated the entire height of the reservoir. Also, the production well is capped on the bottom to prevent infiltration of formation sand.

## Sand Tank Production Well

**Sand Tank**
**East Baton Rouge Parish, LA**

**OBJECTIVE** **Production Well Experimental Data**

| WELL INFORMATION | | | | |
|---|---|---|---|---|
| Sand Tank Well ID | 1 | | | |
| Working Interest / Net Revenue Interest | 100% / 100% | | | |
| Lease Location | LSU | | | |
| Well Type | Experimental | | | |
| Project Type | Sand Tank Experiment | | | |
| Deviations (KOP / Max / Zonal) | Straight Hole | | | |
| **RESERVOIR INFORMATION** | | | **Current** | |
| Reservoir | Sand Tank Reservoir | Type: | Water - Medium Grain Sand | |
| Gross Sand | 1.5 ft (' to ' MD) | | Mid-zone | |
| Net Pay | 1.5 ft | | 0.75' MD | |
| Porosity / Permeability | 0.35 % / 60000 md estimated | | | |
| TVD Perforation Interval | 0'-1.5' MD | | | |
| Perforating Information | Slot | | | |
| Phasing | 90 deg | | | |
| Hole Diameter | 0.01 in | | | |
| BHP | .433 psi psi original | ppge | | |
| PVT — Gas Gravity / Oil Gravity | / API | Partial Pressures | Date Tested | 1/0/00 |
| Water Salinity | ppm | $H_2S$ 0 psia | | |
| Mole % $CO_2/N_2/H_2S$ | / / | $CO_2$ 0 psia | Drive Mechanism | |
| Production data — Current Pressures (TP/CP) | psi / 0 psi | | Depletion | |
| (Gas/Oil/Water) | mcfd / 0bopd / 8.57bwpd - | | Date Tested | 10/2/11 |

**TUBULAR INFORMATION**

| Description Size | Weight (lbs/ft) | Grade | ID (Inches) | Drift (Inches) | Thread Collar OD | Burst (psi) | Collapse (psi) | Yield (Mlbs) | Capacity (BBL/ft) | Depth |
|---|---|---|---|---|---|---|---|---|---|---|
| Production Casing 2" | 0.4# | PVC | 1.750 | NA | NA | 280 | 300 | NA | 0.00298 | 1.5' |

Figure 5.6: Wellbore information sheet. Pictured above is the information sheet for the wellbores located within the sand tank. All the PVC pipe specifications are included as well as some of the reservoir information. This is representative of the same wellbore information sheets used in industry.

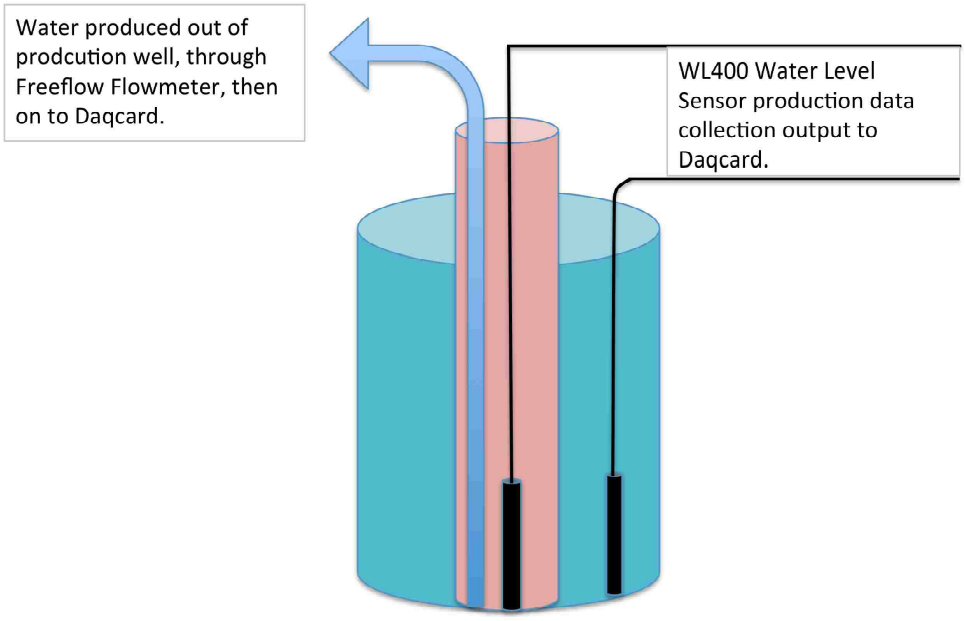


Figure 5.7: Skin test experimental setup. Pictured above is the setup of the PVC "skin" test experiment. For this experimental setup, the production well was placed in a five gallon bucket with a constant water source flowing. While producing water from the well inside the bucket, the pressure inside and outside the well was recorded as well as the flow rate during the production period. The data was then analyzed and a skin factor was determined, in standard US units, from the following equation from (Horne 1995).

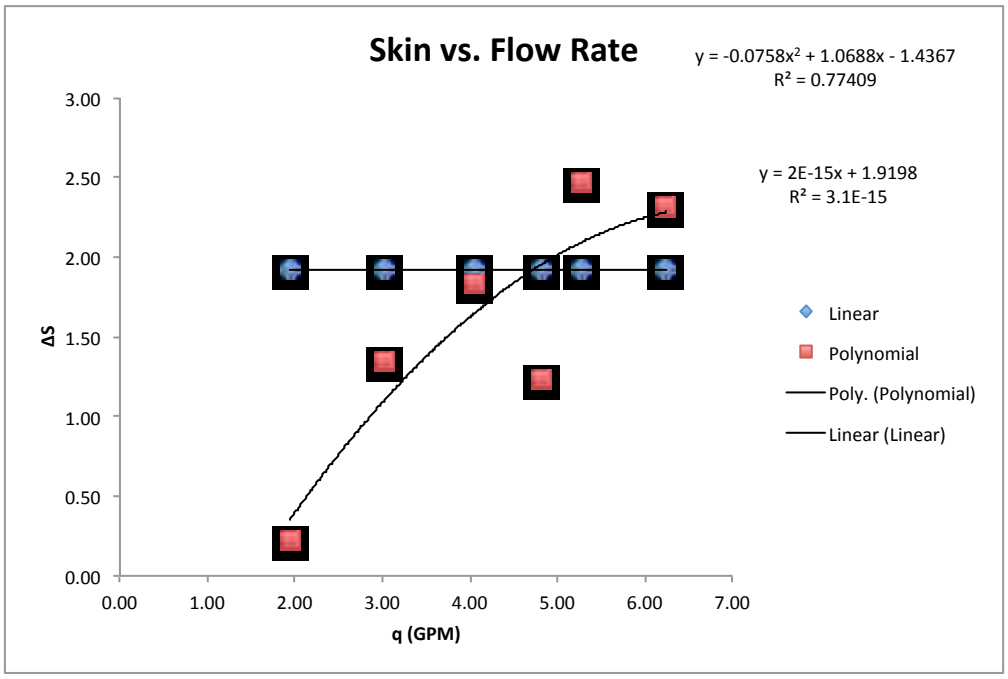


Figure 5.8: Skin vs. flow rate. Pictured in the plot above are the skin effects for both linear and polynomial cases as presented in chapter 4 (Fig. 4.4). For the linear case, as expected, the skin is constant at all flow rates. However, for the polynomial case, the skin is dependent on the flow rate. This is of interest because this is not the case in most real world well completions.

### 5.1.3 WL400 Water Level Sensor Calibration

The WL400 water level sensors located inside each monitoring well, and in the free water side of the tank, are used to make accurate and precise measurements of the water level at each respective location. The sensors were all placed in a five gallon bucket with the controlled water depth at one foot approximately. Then water level readings were taken for ten minutes, at five second intervals, to test both the accuracy and the precision of the instrumentation (Fig. 5.9 & 5.10). An in depth statistical analysis was also performed on the calibration test data using Rose and Associates software (Fig. 5.11 & 5.12).

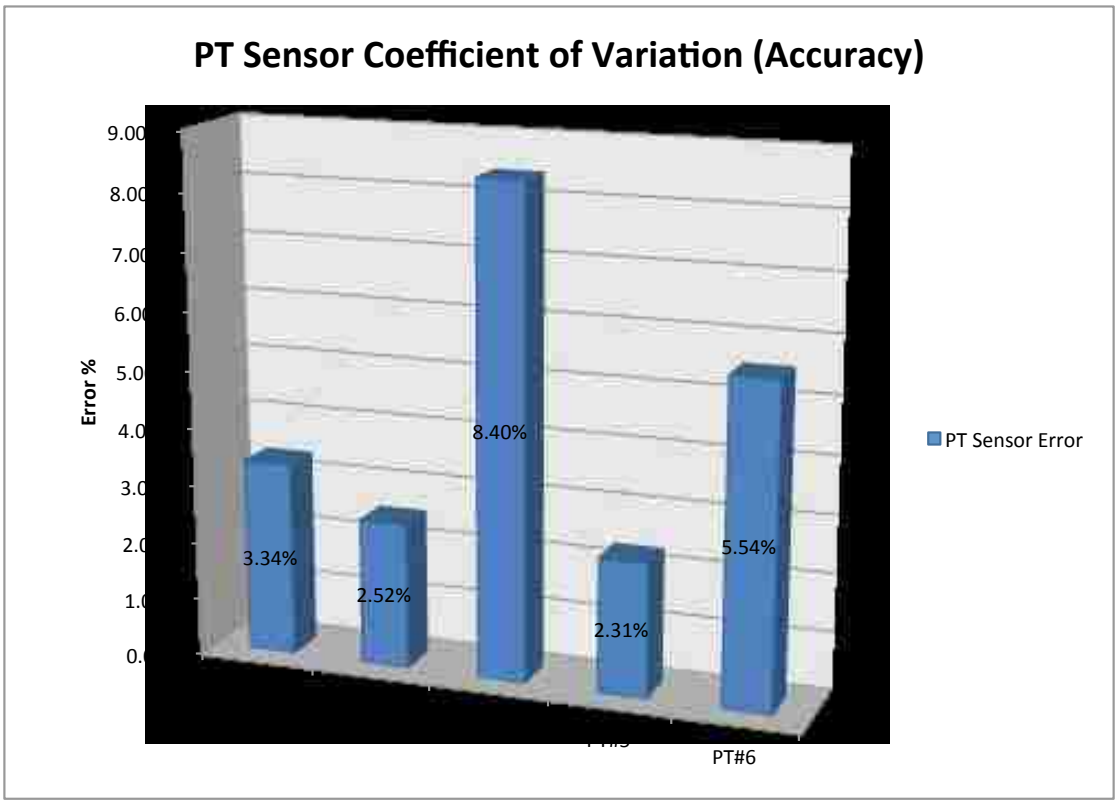


Figure 5.9: Accuracy of the WL400 water level sensors. Illustrated above is the accuracy of the WL400 water level sensors as calculated from experimentation. The sensors were all placed in exactly one foot of water and readings were taken every five seconds for ten minutes. Sensors 1,2, and 5, are adequate enough for experimentation but sensors 3 and 6 should be re-calibrated.

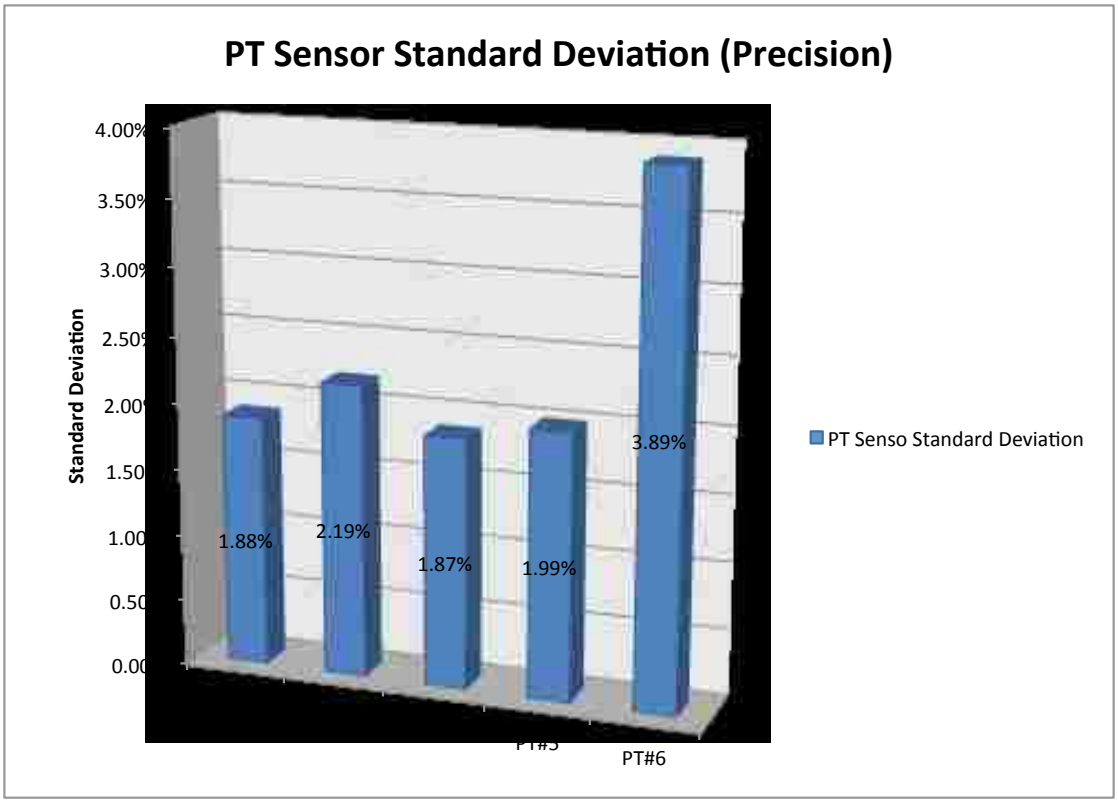


Figure 5.10: Precision of the WL400 water level sensors. Illustrated above is the precision of the WL400 water level sensors as calculated from experimentation. The sensors were all placed in exactly one foot of water and readings were taken every five seconds for ten minutes. The precision of the sensors is greater than the accuracy, however, that is to be expected.

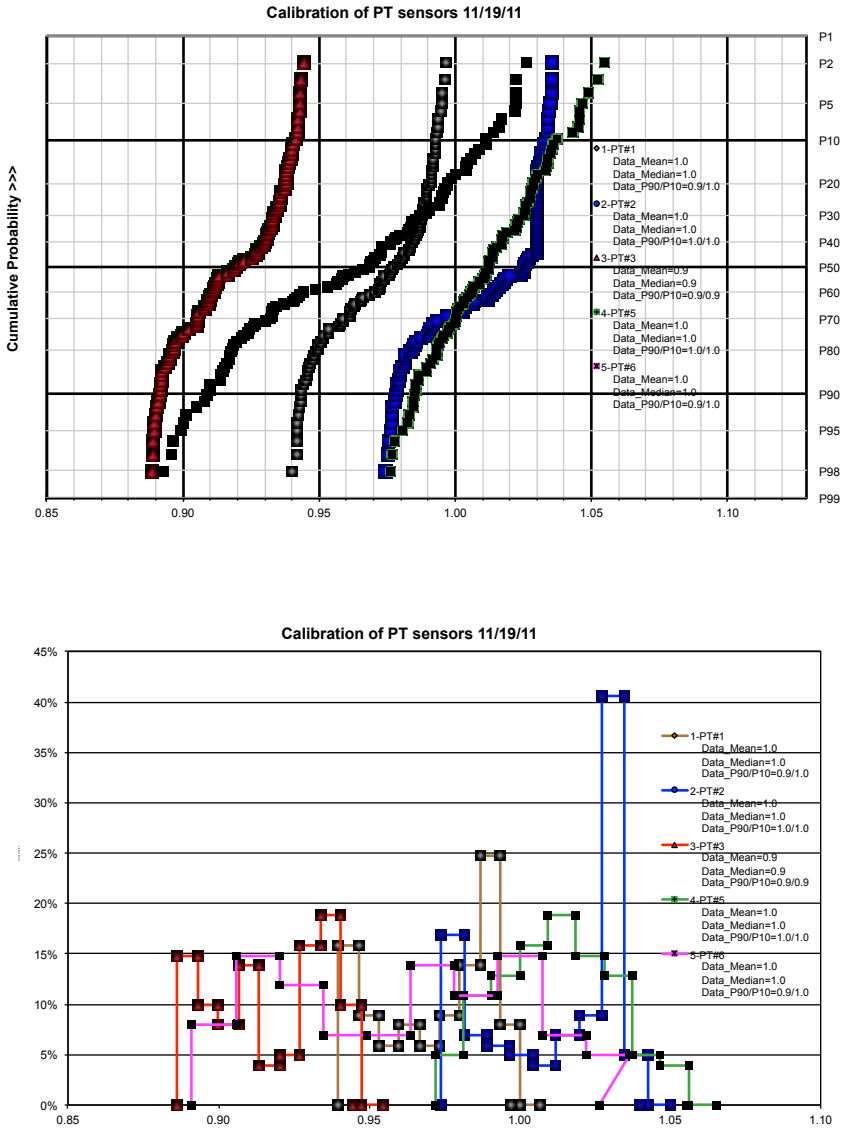


Figure 5.11: Probabilities of WL400 water level sensors. Shown above are the cumulative probability and the probability density of the WL400 water level sensors used in the sand tank experiment. The measurements were taken in approximately one foot of water. The plots further substantiate the great degree of precision possessed by the WL400 water level sensors.

**R&A Enhanced Plotting System - Numerical Results and Statistics**

| | Statistics | Group 1 | Group 2 | Group 3 | Group 4 | Group 5 |
|---|---|---|---|---|---|---|
| Input Data Set | Is this Group being plotted? | Active | Active | Active | Active | Active |
| | Description of group | PT#1 | PT#2 | PT#3 | PT#5 | PT#6 |
| | Valid data points (only numeric data with a positive value) | 101 | 101 | 101 | 101 | 101 |
| | Minimum data value | 0.94 | 0.97 | 0.89 | 0.97 | 0.89 |
| | Maximum data value | 1.00 | 1.04 | 0.94 | 1.06 | 1.03 |
| Input Data Stats | P99 | 0.94 | 0.97 | 0.89 | 0.98 | 0.89 |
| | P90 | 0.94 | 0.98 | 0.89 | 0.99 | 0.91 |
| | P50 (median) | 0.98 | 1.03 | 0.92 | 1.01 | 0.97 |
| | **Mean (simple arithmetic)** | **0.97** | **1.01** | **0.92** | **1.01** | **0.96** |
| | P10 | 0.99 | 1.03 | 0.94 | 1.04 | 1.01 |
| | P1 | 1.00 | 1.04 | 0.94 | 1.05 | 1.03 |
| Lognormal Best Fit Curve | P99 | 0.93 | 0.96 | 0.87 | 0.96 | 0.87 |
| | P90 | 0.95 | 0.98 | 0.89 | 0.99 | 0.91 |
| | P50 (median) | 0.97 | 1.01 | 0.92 | 1.01 | 0.96 |
| | **Truncated Mean (P1>P99)** | **0.97** | **1.01** | **0.92** | **1.01** | **0.96** |
| | P10 | 1.00 | 1.05 | 0.94 | 1.04 | 1.01 |
| | P1 | 1.02 | 1.07 | 0.97 | 1.06 | 1.06 |
| Other | Legend text (editable) | Data_Mean=1.0<br>Data_Median=1.0<br>Data_P90/P10=0.9/1.0 | Data_Mean=1.0<br>Data_Median=1.0<br>Data_P90/P10=1.0/1.0 | Data_Mean=0.9<br>Data_Median=0.9<br>Data_P90/P10=0.9/0.9 | Data_Mean=1.0<br>Data_Median=1.0<br>Data_P90/P10=1.0/1.0 | Data_Mean=1.0<br>Data_Median=1.0<br>Data_P90/P10=0.9/1.0 |

Figure 5.12: Statistical analysis of the WL400 water level sensors. Illustrated above are numerical results and statistics for the five water level sensors used in the experiment. As shown in the previous figures 5.9 and 5.10, the sensors are more precise than accurate. This goes to reason and shows that the sensors can be more accurate with appropriate recalibration. It is also important to note, the sensors are very sensitive and should be handled with great care. During experimentation a sensor was damaged and is currently being sent to the manufacturer for repair.

### 5.1.4 FreeFlow P-Type Flow Transmitter Calibration

As previously stated, the flowmeter that was used in this experimentation is factory calibrated to be accurate in the 5-15 gpm range. However, for the experiment being ran, a flowmeter with accuracy in the 0-1 gpm range is necessary. As a result, the production flow rates for this experimental run had to be hand set and are inaccurate. It is recommended that for further experimentation another flowmeter calibrated to the correct flow range be used. As shown in Figure 5.13, the current flow transmitter is inaccurate to a degree that is not desirable for use in this experiment.

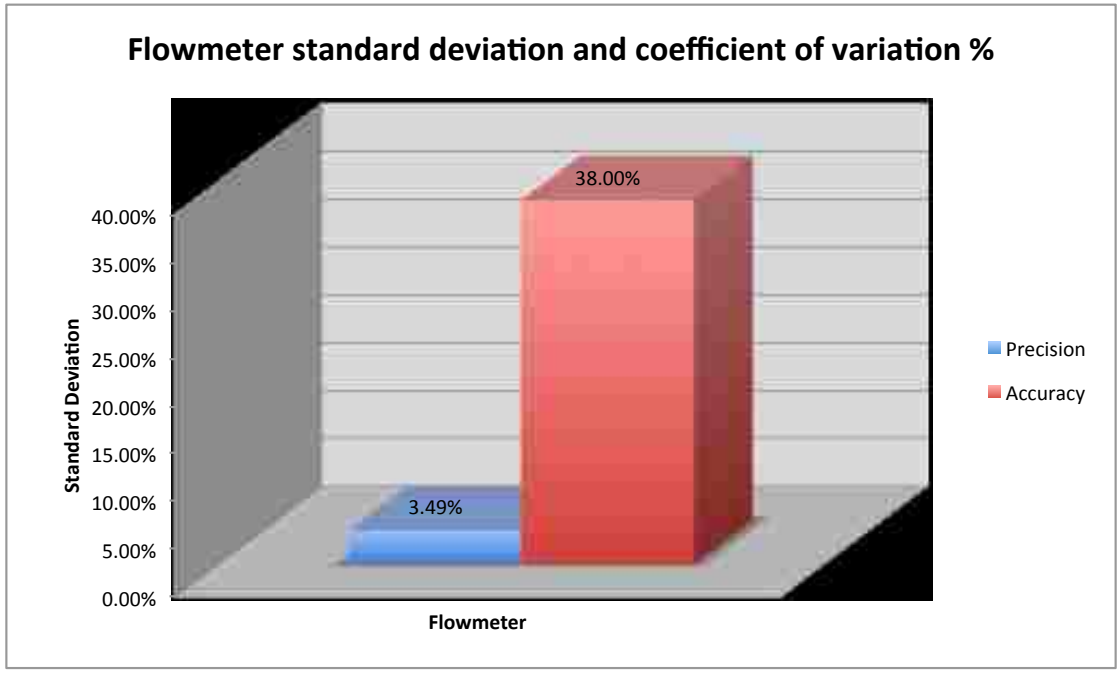


Figure 5.13: Precision and accuracy of the flowmeter. Illustrated above are the standard deviation and coefficient of variation for the precision and accuracy of the FreeFlow P-Type Flow Transmitter. The transmitter is, as discussed, a great deal more precise than accurate in the ranges of flow measured for this experiment. This shows the transmitter inaccuracy and therefore substantiates reason another transmitter should be used in future experimentation.

### 5.1.5 Seismic Equipment Calibration

All of the seismic equipment built and used in this experiment was initially calibrated and tested by Dr. Juan Lorenzo's group. If it is necessary to verify specific calibration techniques used refer to the calibration section of the Smolkin (2011)

Thesis. The equipment was originally calibrated in a small box full of sand, Figures 5.14 & 5.15, and later moved to the sand tank for additional calibration.

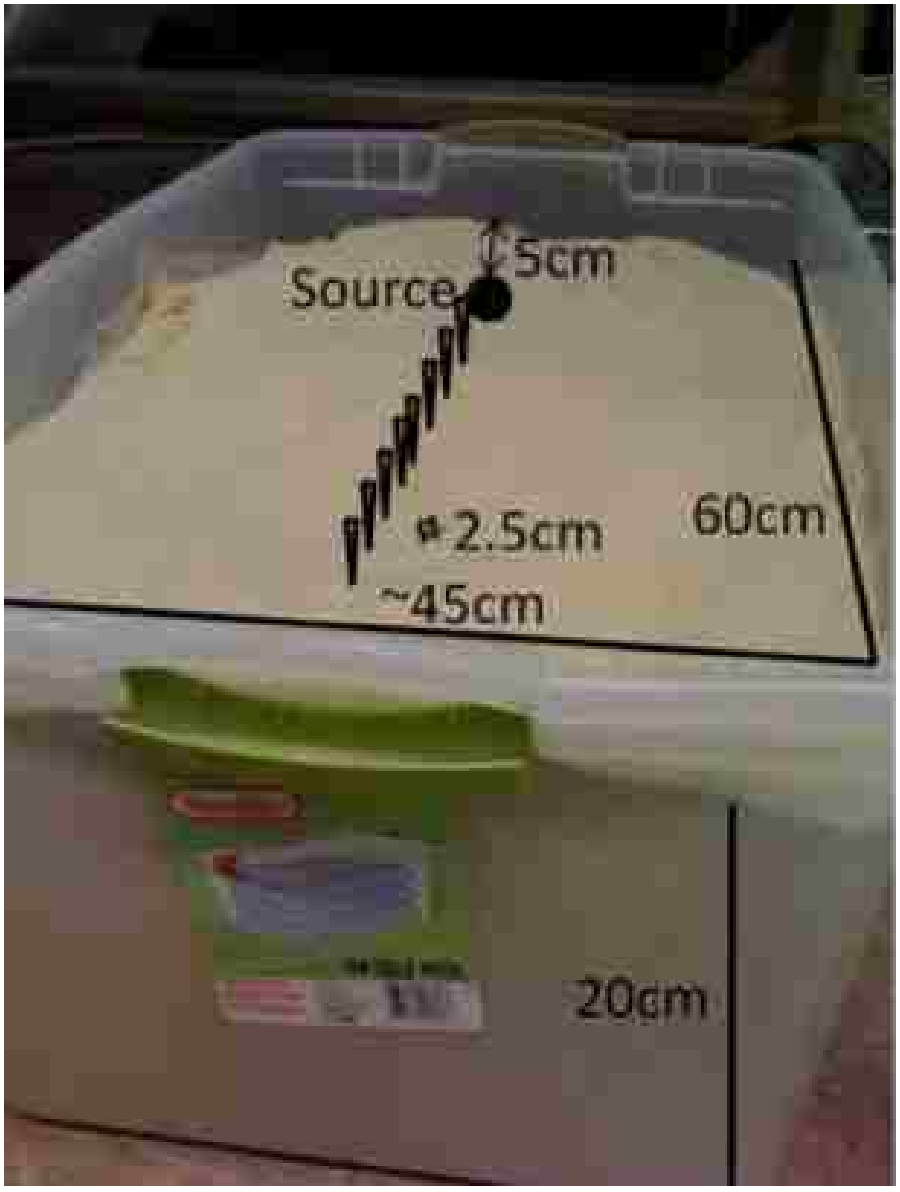


Figure 5.14: Seismic calibration sandbox. Initially, a sandbox is used by Smolkin (2011) to test whether the acquisition system receives appropriate signals. The sandbox measures 25 cm by 60 cm and is filled with 25 cm of sand. Due to the small size and shallow depth of sand in the box, edge effects are unavoidable and are observed in the results. Dimensions of sandbox filled with dry play sand and schematic display of source (circle) and receiver (long spike shapes) geometry (Smolkin 2011).

As a point of interest it should be mentioned that a significant amount of noise in the data results from misplacement of position and orientation of the sensors.

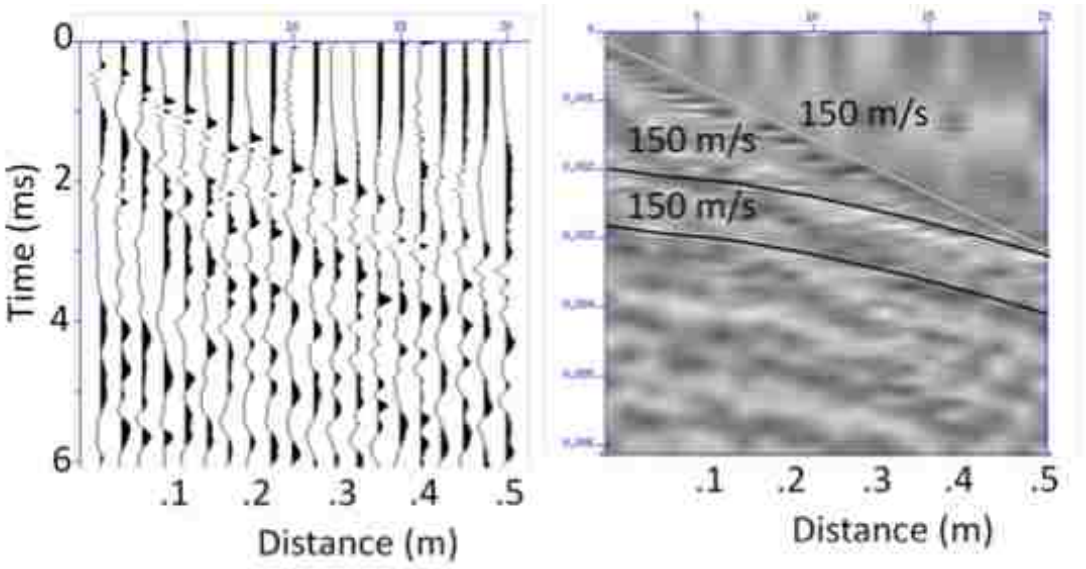


Figure 5.15: Initial shot gathers from seismic calibration sandbox. Seismic gather of the experiment conducted in dry sand. Filter parameters are: 200,400,10000,15000 Hz and AGC gain uses a 1 ms window. The first interpreted reflection is from the walls of the box. The second reflection comes from the bottom of the box (Smolkin 2011).

Furthermore, orientation is difficult to maintain in the dry sand because the tension of the thick black wires that carry the power and the signal to and from the sensors have a tendency to twist and pull the sensors despite efforts to seat them properly (Smolkin 2011). Also, there is always some residual saturation in the sand pack, even when the tank is completely drained and no water is present.

## 5.2 Test Runs

In April 2011, some preliminary data for the sand tank experiment was collected. This was the first run of the experiment with all necessary production as well as seismic data collection equipment working properly. Data includes production data collection as well as all seismic data collection equipment locations. This data is based on a 2-D depiction of the top of the sand tank in $x$ and $y$ coordinates as shown in Figure 5.1. The production data is collected for the experimental run by monitoring well number and time interval is also included and shown (Fig.5.16). Finally, the seismic data was collected and processed from the run (Fig.5.17) and was found suitable for use in the experimentation with the help of the geophysical experts.

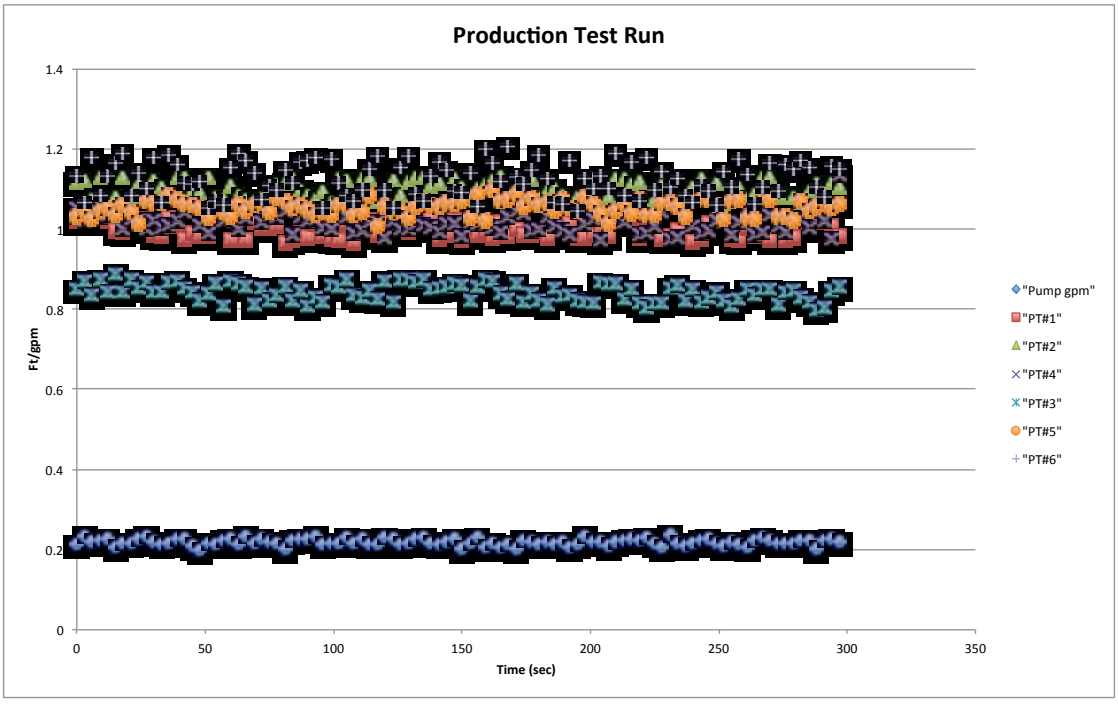


Figure 5.16: Preliminary production data collection. Pictured above is the preliminary production data from the initial data collecting run of the sand tank experiment. All six PT sensors are present as well as pumping rate in GPM. The head in the production well is steady at approximately .8 ft while the pump is producing at approximately .25 GPM

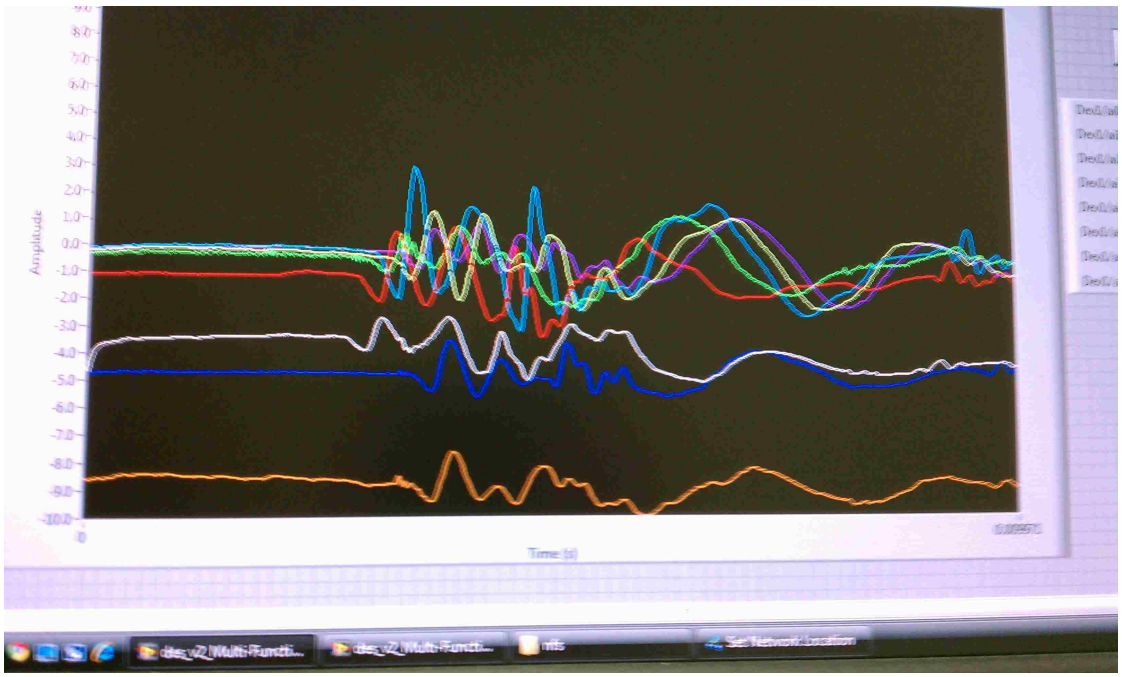


Figure 5.17: Seismic data collection in Labview. Pictured above are the seismic data first arrival times. This is an example of the images captured in the log view data acquisition module for the seismic arrivals in the sand tank experiment. All 8 accelerometers are collecting first arrival data. The white line is closest to the source and shows first arrival soonest while the dark blue line is furthest from the source and shows first arrival latest.

## 5.3 Full Experimental Run

In October of 2011, a full scale experiment was run in the sand tank. This was the first ever full scale experiment run in the sand tank and includes all necessary production and seismic data. The configuration of all equipment locations is depicted in a 2-D representation of the top of the sand tank in $x$ and $y$ coordinates as shown in Figure 5.1. The only difference is that PT sensor #4 was inoperable, so PT sensor #5 was moved to the former location of PT sensor #4, and there was no PT sensor in the former location of PT sensor #5. The eight accelerometers are buried approximately 1 cm below the sand surface and placed about .5 cm apart, for a total length of 12 cm. The first shot point was 12 cm in the positive y direction, shown in Figure 5.1, from receiver 1. Each following shot was moved out 12 cm for a total length of 96 cm over 8 shots.

The first task was to set up the experiment as explained in chapter four. After the setup was complete, all equipment was tested for proper function and calibration as explained earlier in this chapter. A seismic survey was conducted before adding any water to the tank. This was done to act as a control for the later seismic surveys, in which water would be present in the tank. After processing the preproduction, dry tank, seismic data as prescribed in chapter four, it is possible to get a feel for the internal structure of the sand tank. Note, the frequency filter parameters used for all seismic processing in this experimental run are: 1500,3000,8000,16000 Hz and AGC gain uses a 1 ms window as prescribed by Smolkin (2011).

As shown in Figure 5.19 there appears to be two separate refractive layers, as well as a possible third layer interpreted using reflected arrivals, within the sand tank. The velocity of the first layer of the tank is estimated to be 150 m/s, while the velocity in the second layer is estimated to be 160 m/s. For all the velocity models interpreted, the maximum velocity in the sand appears to be 220 m/s and the minimum is 100 m/s (Smolkin 2011). Also, Smolkin (2011) was able to interpret a third layer using refracted arrivals, with a fourth possible layer interpreted using the reflected arrivals. This experiment was not able to reproduce a third layer using refracted arrivals possibly because the sand within the tank was disturbed when installing several monitoring wells for the experiment.

As mentioned previously, in the calibration section of this chapter, it is necessary to let the water sit in the tank some time before it comes to equilibrium conditions fit to run the experiment. So after the tank was filled with water, the tank was left to sit for seven hours for equilibrium to be achieved. After the tank was filled with water and came to equilibrium, another seismic survey was shot with approximately one foot of water in the tank. This was done to compare not

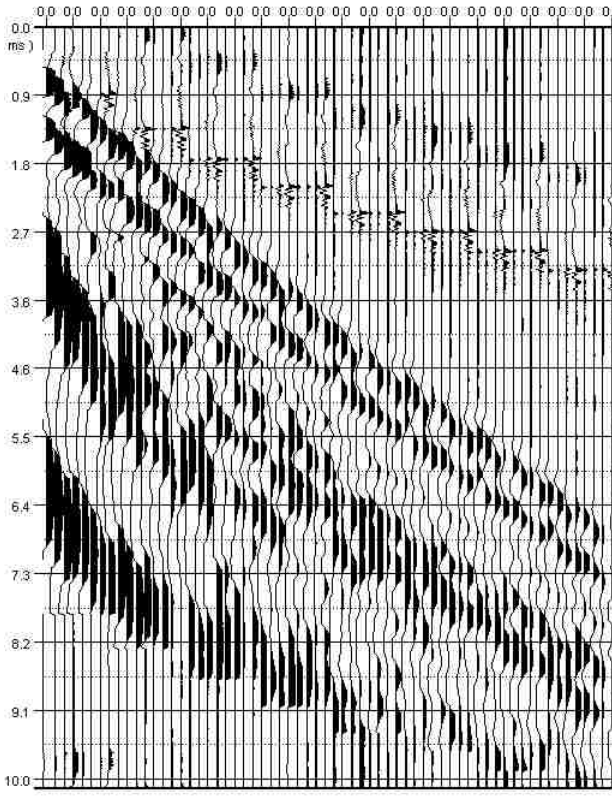


Figure 5.18: Wiggle plot of dry sand tank. Pictured above is a wiggle plot of the sand tank with no water added. The vertical scale is in microseconds and the horizontal scale is in meters, similar to figure 5.19. Present in the wiggle plot are what appears to be two separate velocity layers, some surface waves, and what appears to be some noise from the collection equipment. A seismic survey was done on the dry tank as a control.

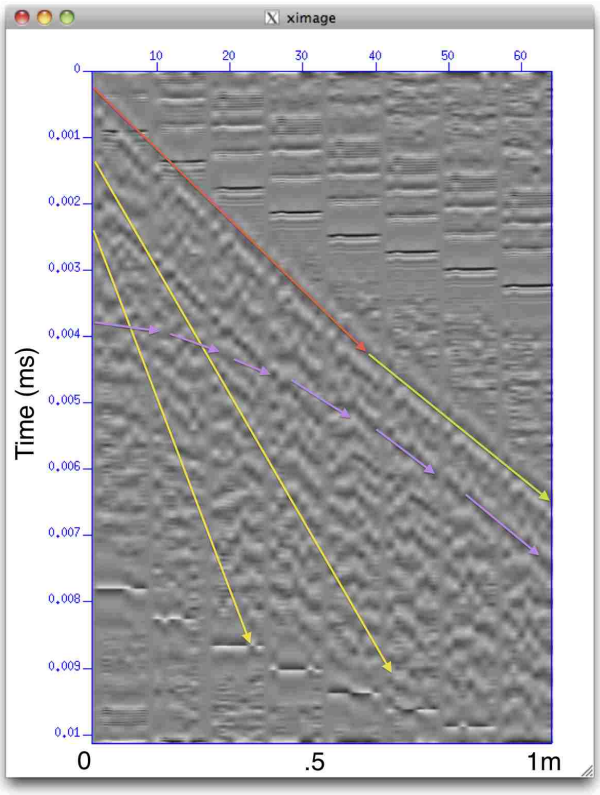


Figure 5.19: Image plot of dry sand tank. Pictured above is an image plot of the sand tank with no water added. The first layer arrivals are indicated in red, the second layer in green. The reflections from the bottom of the tank in purple, and the surface waves in yellow. The eight horizontal lines present in the figure are due to the shifting script developed by (Smolkin 2011) used on the seismic data as described in chapter four.

only with the seismic survey of the dry tank but also to compare with the seismic surveys of the tank while water production was occurring.

As shown in Figure 5.21, there appears to be two separate refractive layers, as well as a possible third and fourth layer interpreted using reflected arrivals, within the sand tank. The velocity of the first layer of the tank is estimated to be 125 m/s, while the velocity in the second layer is estimated to be 167 m/s. It is important to mention that velocities in the range of 1500 m/s, which indicates full water saturation, are never realized. This is due to the sand tank never reaching one hundred percent saturation due to capillary forces as discussed in chapter four and also in Smolkin (2011).

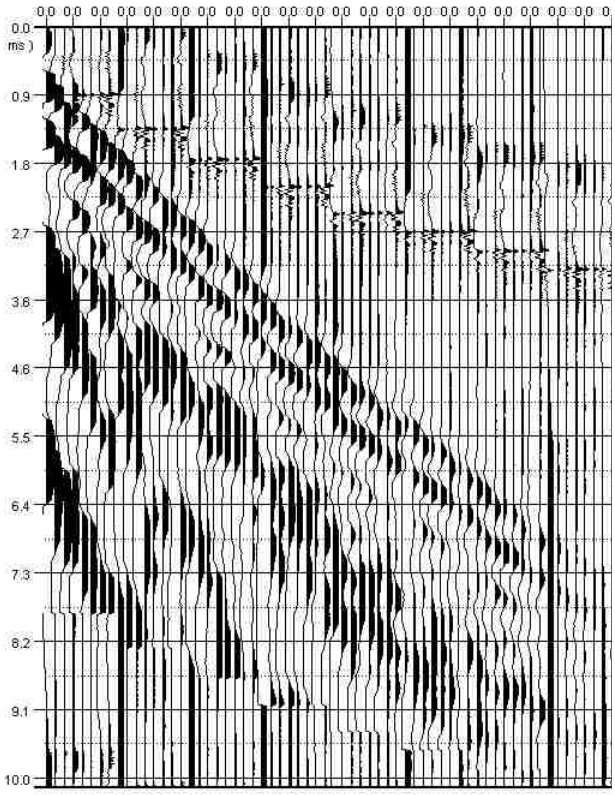


Figure 5.20: Wiggle plot of full sand tank. Pictured above is a wiggle plot of the sand tank filled with a foot of water. The vertical scale is in microseconds and the horizontal scale is in meters, similar to figure 5.21. Present in this wiggle plot are what appears to be two separate layer first arrivals, clear presence of surface waves, and what appears to be some noise from the collection equipment.

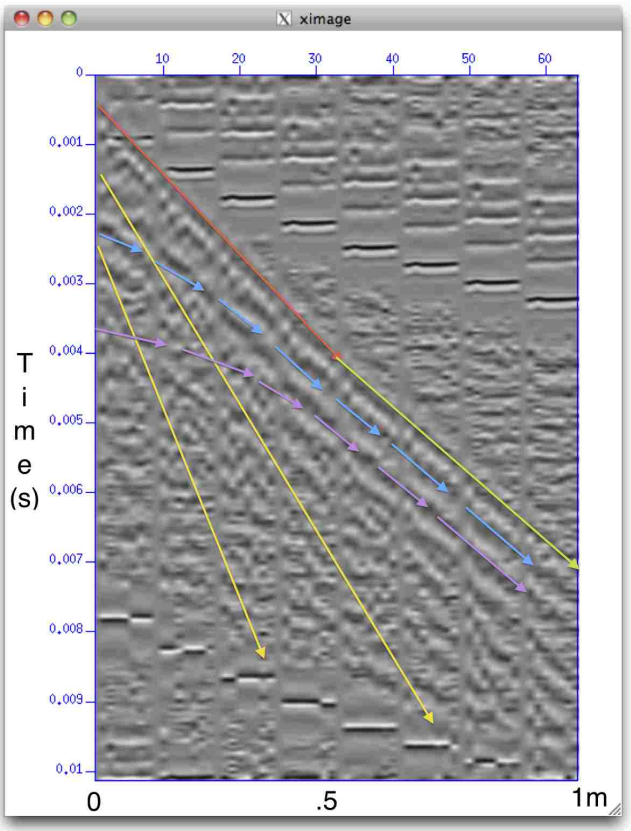


Figure 5.21: Image plot of full sand tank. Pictured above is an image plot of the sand tank filled with a foot of water. The first layer arrivals are indicated in red, the second layer in green. The reflections from the capillary fringe are indicated in blue, the reflections from the bottom of the tank in purple, and the surface waves in yellow.

The next step was to start water production from the sand tank. This was performed as per instructions in chapter three of this document. Illustrated in Figure 5.22 is the sand tank production data for this experimental run. There is over fifteen hours of sand tank production data collected in Daqview. The production data show the water starts at an average depth in the sand tank of one foot and declines to an average depth of 0.83 feet after fifteen hours of production. The data also show that the water in being produced at an average of 0.25 gpm over the fifteen hour production interval. As plotted in purple, PT sensor number 3, is the pressure and temperature sensor in the producing well. It behaves erraticly at first and then settles down after a couple hours. Also to be noted is that the water depth inside the production well is increasing rather than decreasing over time as shown in all other monitoring wells in the experiment. This will be discussed in some detail later in chapter six.

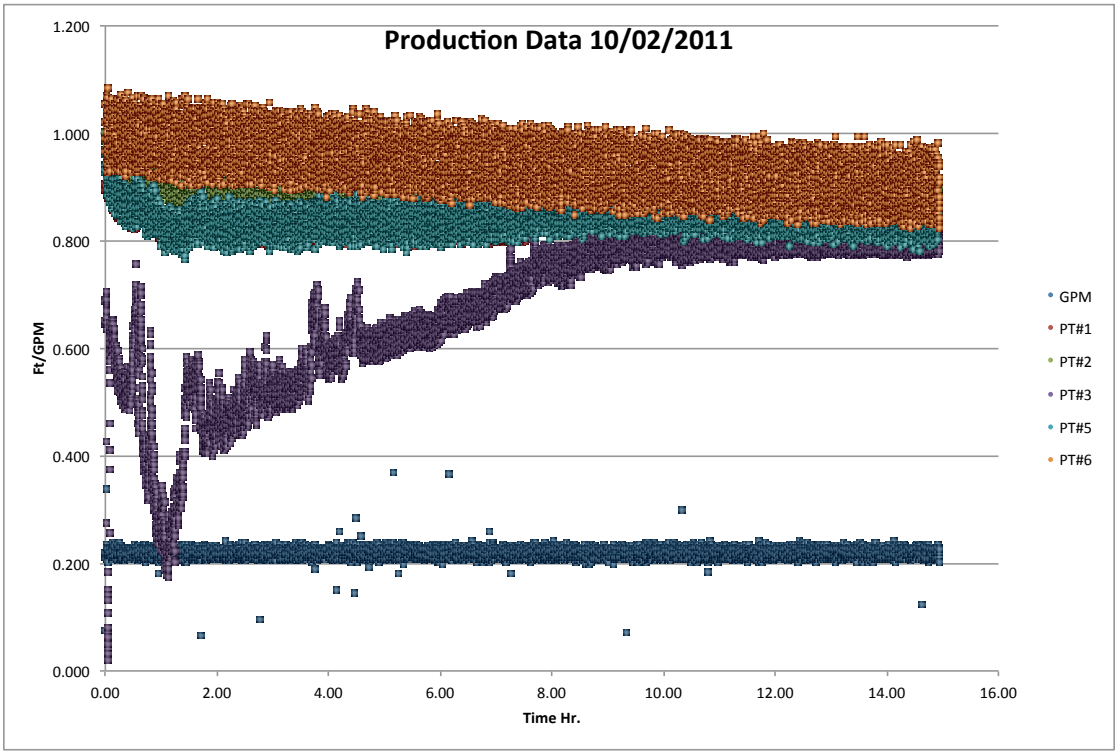


Figure 5.22: Experimental production data recorded in Daqview. Pictured above is the production data from the full run of the sand tank experiment on October 11, 2011. As shown above water was produced from the sand tank, and experimental data was collected, for more than 15 hours. During this production period, three seismic surveys were taken. Two additional seismic surveys were performed prior to producing water from the sand tank to be used as controls for this experiment, one dry tank survey and one full tank non-production survey.

After producing water from the sand tank for approximately one hour a third seismic survey was shot. As shown in Figure 5.24, there appears to be two

separate refractive layers, as well as a possible third and fourth layer interpreted using reflected arrivals, within the sand tank. The velocity of the first layer of the tank is estimated to be 125 m/s, while the velocity in the second layer is estimated to be 167 m/s. It is important to mention that velocities in the range of 1500 m/s, which indicates full water saturation, are still not realized.

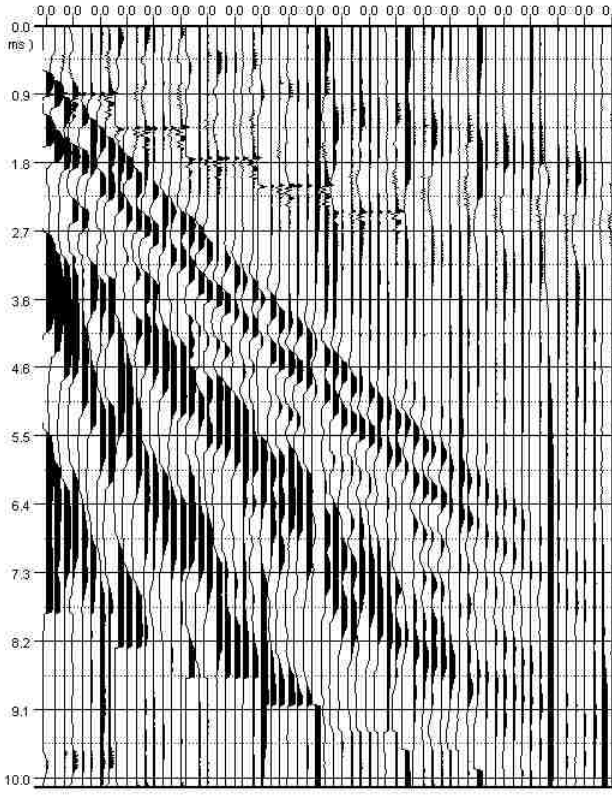


Figure 5.23: Wiggle plot of sand tank during production survey 1. Pictured above is a wiggle plot of the sand tank after producing water for approximately one hour. The vertical scale is in microseconds and the horizontal scale is in meters, similar to figure 5.24. Present in this wiggle plot are what appears to be two separate layer first arrivals, clear presence of surface waves, and what appears to be some noise from the collection equipment.

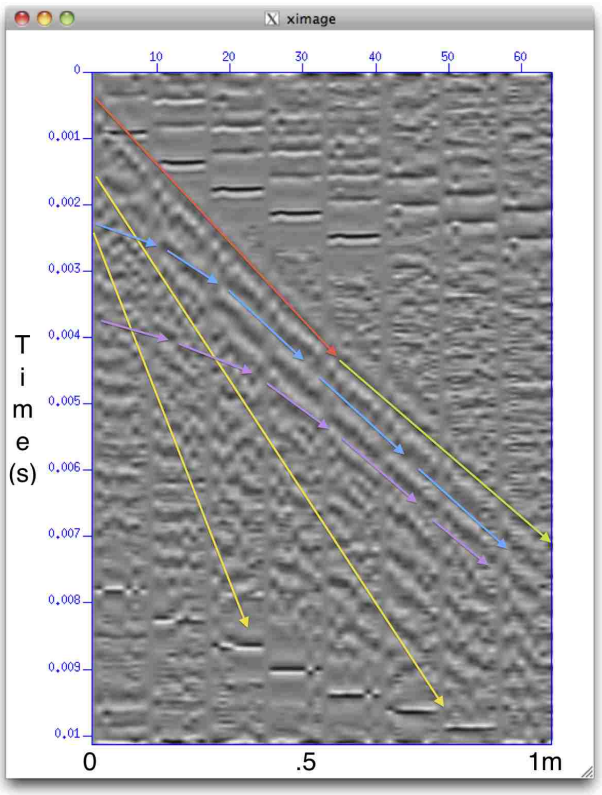


Figure 5.24: Image plot of sand tank during production survey 1. Pictured above is an image plot of the sand tank while producing water. This survey was taken approximately one hour after water production started in the tank. The first layer arrivals are indicated in red, the second layer in green. The reflections from the capillary fringe are indicated in blue, the reflections from the bottom of the tank in purple, and the surface waves in yellow.

After producing water from the sand tank for approximately five hours a fourth seismic survey was shot. As shown in Figure 5.26, there appears to be two separate refractive layers, as well as a possible third and fourth layer interpreted using reflected arrivals, within the sand tank. The velocity of the first layer of the tank

is estimated to be 125 m/s, while the velocity in the second layer is estimated to be 167 m/s. It is important to mention that velocities in the range of 1500 m/s, which indicates full water saturation, are still not realized.

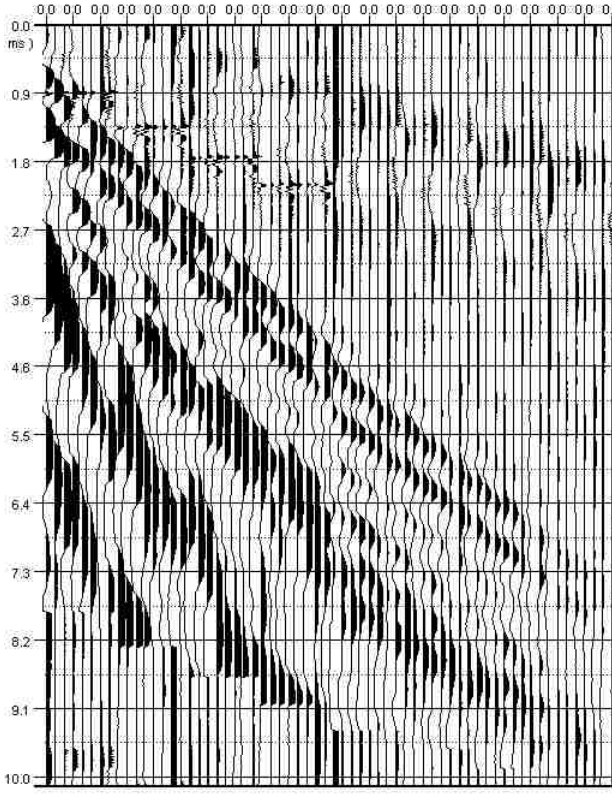


Figure 5.25: Wiggle plot of sand tank during production survey 2. Pictured above is a wiggle plot of the sand tank after producing water for approximately five hours. The vertical scale is in microseconds and the horizontal scale is in meters, similar to figure 5.26. Present in this wiggle plot are what appears to be two separate layer first arrivals, clear presence of surface waves, and what appears to be some noise from the collection equipment.

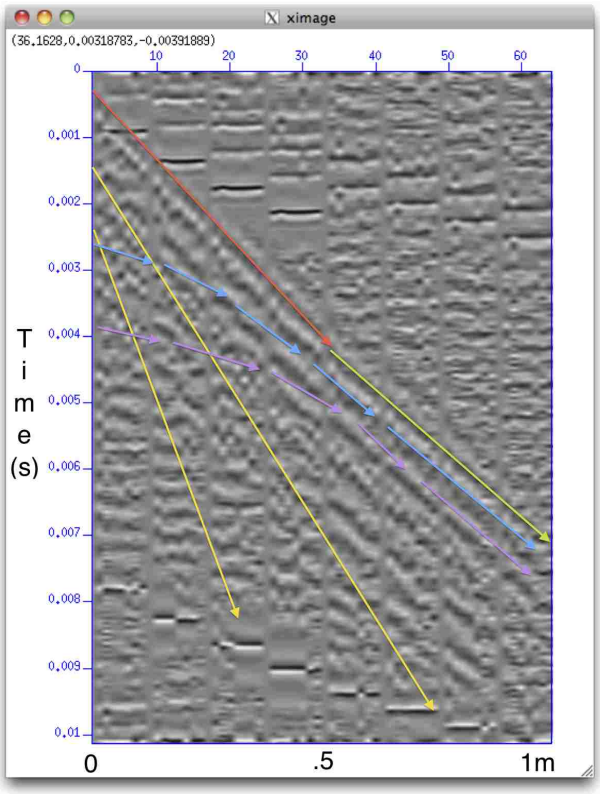


Figure 5.26: Image plot of sand tank during production survey 2. Pictured above is an image plot of the sand tank while producing water. There are two layers present, the apparent velocities of layer one and two are 125 m/s and 167 m/s respectively. The first layer arrivals are indicated in red, the second layer in green. The reflections from the capillary fringe are indicated in blue, the reflections from the bottom of the tank in purple, and the surface waves in yellow.

After producing water from the sand tank for approximately fifteen hours a fifth, and final, seismic survey was shot. As shown in Figure 5.28, there appears to be two separate refractive layers, as well as a possible third and fourth layer interpreted using reflected arrivals, within the sand tank. The velocity of the first layer of the tank is estimated to be 125 m/s, while the velocity in the second layer

is estimated to be 167 m/s. It is important to mention that velocities in the range of 1500 m/s, which indicates full water saturation, are still not realized.

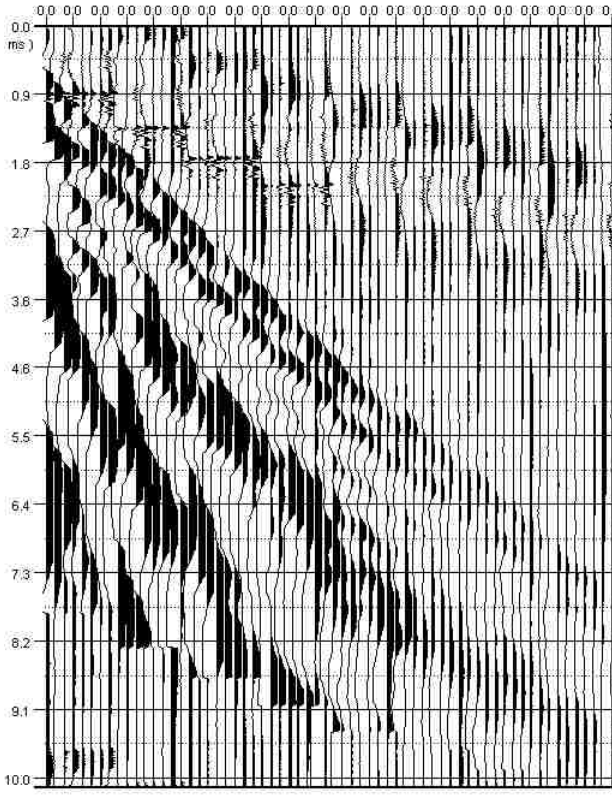


Figure 5.27: Wiggle plot of sand tank during production survey 3. Pictured above is a wiggle plot of the sand tank after producing water for approximately fifteen hours. The water level in the sand tank has went from an average of one foot to and average of .83 feet over the five sensors in the tank. The vertical scale is in microseconds and the horizontal scale is in meters, similar to figure 5.21. Present in this wiggle plot are what appears to be two separate layer first arrivals, clear presence of surface waves, and what appears to be some noise from the collection equipment.

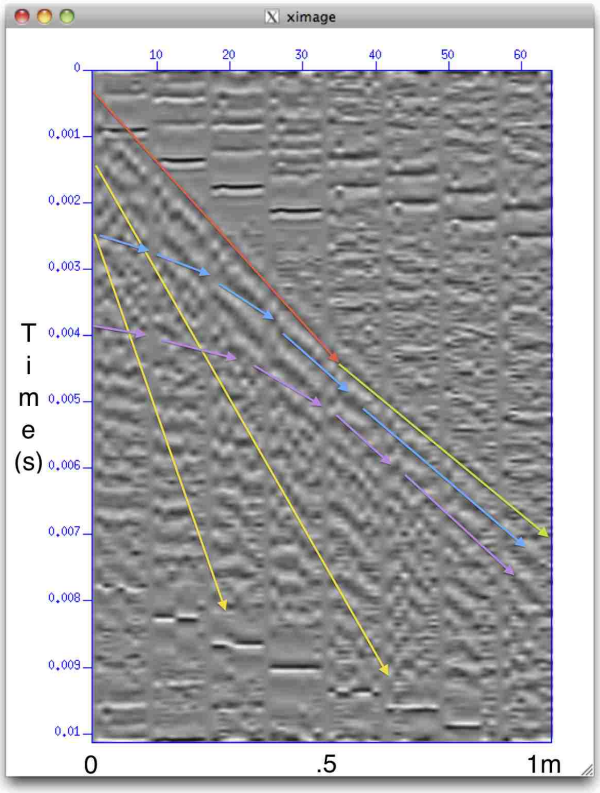


Figure 5.28: Image plot of sand tank during production survey 3. Pictured above is an image plot of the sand tank while producing water. The velocity of the first layer of the tank is estimated to be 125 m/s, while the velocity in the second layer is estimated to be 167 m/s. Velocities in the range of 1500 m/s, which indicates full water saturation, are still not realized. The first layer arrivals are indicated in red, the second layer in green. The reflections from the capillary fringe are indicated in blue, the reflections from the bottom of the tank in purple, and the surface waves in yellow.

When the collection of the production data and all five seismic surveys was concluded and processed, it was then necessary to perform a first break picking routine on the seismic traces. This must be done to enable comparison with the first arrival times calculated by rayinvr using the velocity model created by the

simulation data. To perform this routine it was more accurate to use the visual first break picking software in Geogiga front end, as discussed in chapter two. Per Figure 5.29 it is apparent the first arrival times from the survey without water in the sand tank are faster than the first arrivals from the surveys with water present in the tank. Furthermore, the residual between the times increases with distance from the source. Also notice it is apparent there are two different layers represented by the first arrival refractions, further cementing the idea that two separate layers with two different velocities are present within the sand tank.

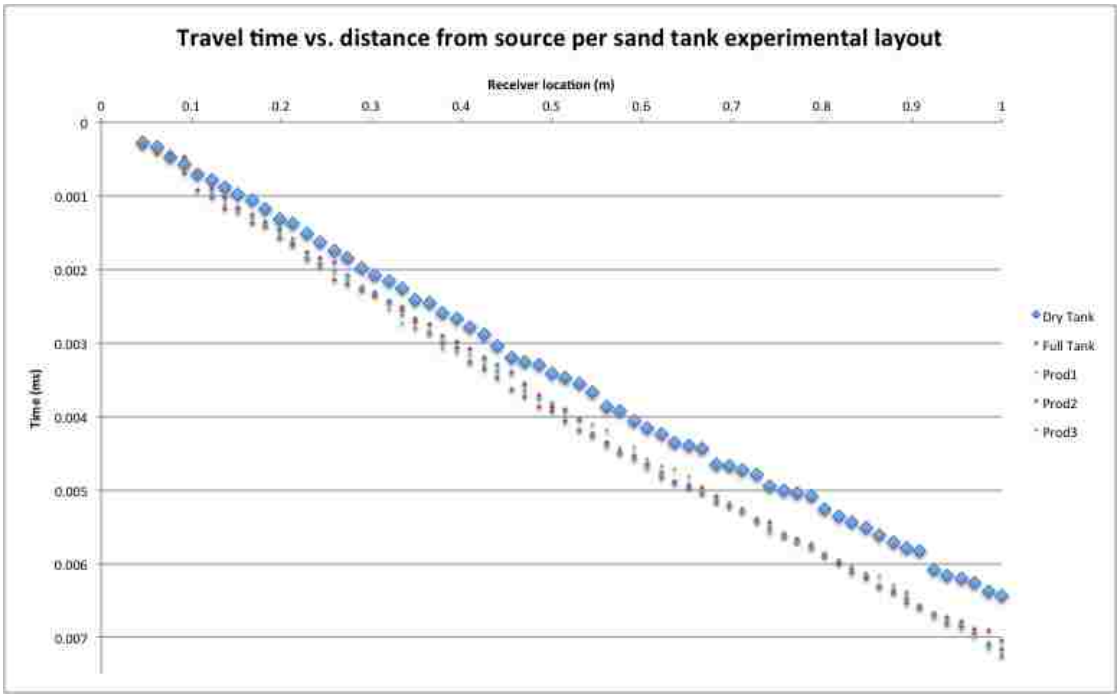


Figure 5.29: First arrival travel time vs. distance from source plot. This is a travel time vs. distance from source plot of the first arrival times per the experimental setup in the sand tank. The first arrival times from the sand tank survey without water arrive before the first arrivals recorded from the sand tank surveys when water is present. This is to be expected, compressional p waves travel slower in partially saturated media, as described by Bachrach and Nur (1998). Also, two distinct layers appear to be present in the sand tank by the apparent change in trend of the first arrivals times at approximately 0.0033 ms.

The first breaks are now picked and ready to be compared to the synthetic arrival times of the simulation process. The observations will be matched against the synthetic calculated data using a parallel implementation of an Ensemble Kalman Filter, commonly referred to as EnKF. After the comparisons are made, simulator conditions can be adjusted until the simulated results match the experimental results to a reasonable measure.

## 5.4 Key Points

- All observation data acquisition equipment was calibrated and a relative error was assigned to the same.
- Test data was collected to assure data quality.
- Full experimental run with production and seismic observation data was completed and analyzed.

# Chapter 6

# Discussion

The experimental setup used in the sand tank is unique to say the least. Few high frequency seismic acquisition systems of the size developed by Smolkin (2011) for this application exist. The seismic acquisition equipment coupled with the production data acquisition equipment prove to be effective in providing useful tools for reservoir surveillance. The degree of the usefulness is of this data is what needs to be determined.

## 6.1 Limitations of Theory

Seismic physical modeling has assumptions and limitations, such as scaling, heterogeneity and reproducibility (Smolkin 2011). The Biot-Gassmann correlations have been proved in highly compacted media and not strongly verified in unconsolidated granular media. It is intended for use in media which has reached a water saturation of 100% and has not been successfully applied to partial saturations (Bachrach and Nur 1998). Because of this, velocities in the sand tank appear to be over estimated by a factor of approximately 4 (Smolkin 2011).

## 6.2 Limitations of Equipment in Experimental Setup

The most pressing limitation of the sand tank experimental setup is improper equipment. The flowmeter used for this experimental run did not accurately measure fluid flow in the ranges needed for this experiment. Therefore, the flowmeter had a relative error which was in the range of 38%. This is unacceptable for future work and must be corrected. Also, the pump used to produce the water from the reservoir must also be upgraded to one that can be more finely tuned to provide flow within the needed ranges of this experimentation.

The second notable limitation of this experimental setup is the absence of complete water saturation in the experimental reservoir. Since water saturation in the tank never reaches 100%, the whole tank acts as a capillary fringe. There is no presence of a zero tension surface detected in this experiment or in the previous experimentation. Water-saturation experiments in the wavetank do not lend themselves to fully-saturated conditions, and thus in theory no high contrast barriers exist. The lack of a high contrast boundary is confirmed in the data, as there are no strong changes in refracted velocities (Smolkin 2011).

## 6.3 Experimental Errors

As with any experiment, there is a certain amount of error expected in the acquisition and interpretation of all collected data. The sand tank experiment is no exception to this rule. In this experiment the errors are going to be calculated and split up into two areas of error estimation:

1. The estimated errors associated with the collection and interpretation of the production data
2. The estimated errors associated with the collection and interpretation of the seismic data

For the error estimation in this experiment the absolute error will be found and then the relative error will be calculated in order to make the errors dimensionless so they can be combined. The absolute error, for example, would have units. The relative error, fractional error, is found by dividing the absolute error by the

original quantity. These errors are then able to be expressed as percentages. The relative error is usually more significant than the absolute error (Babbage 1871). The preferred way to collectively assess errors for this experimentation will be to calculate the relative error and then combine them as follows:

if

$$\triangle z = \triangle x + \triangle y$$

then

$$\triangle z = [(\triangle x)^2 + (\triangle y)^2]^{\frac{1}{2}}$$

where $\triangle x$ and $\triangle y$ are the fractional random errors in $x$ and $y$ and $\triangle z$ is the propagated uncertainty in $z$ (Babbage 1871).

### 6.3.1 Production Acquisition Error Estimation

The production data acquisition equipment used for this experiment has been calibrated and relative errors have been tallied as per information in chapter five. Of course the relative error total is much larger when including the flowmeter, as the flowmeter is not calibrated for the flow ranges present in this experiment. The production data is part of the data that will be used to setup the reservoir simulator. The reservoir simulator will then in turn run simulations that produce data that will be used to create velocity models of the sand tank. Those velocity models, in turn, will be used as input parameters for the ray tracing software rayinvr. The relative error for the production data (Fig. 6.1), coupled with the relative error for the simulations and raytracing routine, is crucial to set expectations for the calculated arrival times to come out of rayinvr.

### 6.3.2 Seismic Acquisition Error Estimation

The seismic data acquisition equipment used for this experiment has been calibrated and relative errors have been tallied as per information in chapter four. The seismic data is the used to compare against the synthetic seismic data calculated from the simulations of the production data. It is of importance to know the relative error of the experimentally collected seismic data to be able to accurately judge the fit of the synthetic seismic data.

| PT#1 | PT#2 | PT#3 | PT#5 | PT#6 | Flowmeter | Total |
|---|---|---|---|---|---|---|
| 3.34% | 2.52% | 8.40% | 2.31% | 5.54% | 38.00% | 39.60% |
| 3.34% | 2.52% | 8.40% | 2.31% | 5.54% | | 11.14% |

Figure 6.1: Production data collection errors. Pictured above are the pressure sensor and flowmeter relative error results. When the flowmeter data is removed, the total relative error decreases substantially. This is of interest because a flowmeter calibrated in the correct flow ranges of this experiment could decrease the relative error dramatically. Also, it is important to mention that for the purposes of this experiment, the production equipment errors will be accounted for separately. That is to say that each individual piece of equipment has it's own error that will be applied to it's own measurement. The errors of the production equipment will not be squared and added together.

There is some expected error in the velocity-depth models caused by instruments and the software used as stated by Smolkin (2011). A relative error of 2% in velocities is expected in near offset arrivals, and 0.2 % in farther offset arrivals. For the purpose of the experimentation, there be be an upper and lower bounds for the relative error, using 2% for the maximum case and 0.2% for the minimum case. There is also expected relative error in hand picking the velocities of refracted arrivals. Smolkin (2011) states, by experience, user error in picking velocity of refracted arrivals is on the order of 7 % (Fig. 6.2). As shown (Fig. 6.3) is the change in water saturation vs. the change in compressional wave velocity at 3.5%, 7%, and 14% relative error. There are two graphs, one plots the change in absolute water saturation units from 0-0.98 and the other plots the change in absolute water saturation units from 0.98-1. The plots show the change as the compressional wave velocity changes from the non-saturated and totally saturated state. Plotted on the 0-0.98 plot is the compressional wave velocity changing by some value, due to water saturation, from the compressional wave velocity at 0 saturation. Conversely, plotted on the 0.98-1, is the change in compressional wave velocity from some value at water saturation equals 1. Each value is bounded by error bars to show the tolerance in the water saturation compared to the error in the compressional wave velocity. This is done because there are two separate slopes in when plotting compressional wave velocity vs. water saturation in low velocity sand based on the Biot (1956b, Biot (1956a, Biot (1962) and Gassmann (1951) predictions (Fig. 2.1). The plots show (Fig. 6.3) that as the change in compressional wave velocity increases the change in water saturation increases as well. Where the two slopes converge, at approximately 0.99 water saturation (Fig. 2.1),the change in water saturation vs. the change in compressional wave velocity will go to infinity. This is possible because the relationship between the water saturation and the compressional wave velocity is not linear.

| Column1 | Velocities | First Break Picks | Total |
|---|---|---|---|
| Maximum | 2.00% | 7.00% | 7.28% |
| Minimum | 0.20% | 7.00% | 7.00% |

Figure 6.2: Seismic data collection errors. Pictured above are the relative errors associated with the seismic data acquisition and first break picking in the sand tank experiment. It is of importance to know the relative error of the experimentally collected seismic data, and first break picks, so as to be able to accurately judge the fit of the synthetic seismic data.

## 6.4 Possible Real World Applications

Although the sand tank experiment is not yet finely tuned and calibrated, it shows a promising future. Perhaps someday this experiment will serve as an analog to several real world cases that need relatively inexpensive, readily verified, and easily manipulated robust data sets. These sand tank experiments could one day provide better tools for reservoir characterization and behavior. Coupling seismic surveys with reservoir behavior could also reduce the need for drilling multiple exploratory wells. Using a couple offset wells for calibration, and exploratory seismic surveys, companies could better predict where to drill the next production well to minimize cost and therefore maximize profit. Differentiation between hydrocarbon and water in reservoirs and the interface that exist between the two is another possible application of this experimentation. Possible future uses might also include detecting overpressure zones to minimize chances of catastrophic blowouts.

## 6.5 Future Work

This first run of the sand tank experimentation, including production and seismic data, proved to be relatively useful in it's ability to be used as a calibration tool for reservoir simulation. Though not perfect, the data collected within this experiment show a promising future for comparison studies. This initial run of the sand tank experiment is simple in nature and can be improved upon in many cases. Saturation meters could be added to the experimentally collected data giving a better image of the saturations within the tank. This could be useful in providing better parameters for the simulations. Another improvement to be made are more accelerometers being added to the experiment so three dimensional seismic processing would be possible. This would allow a better overall picture of the subsurface of the sand tank, therefore improving reservoir characterization parameters for the flow model. The two afore mentioned improvements to the sand tank experiment

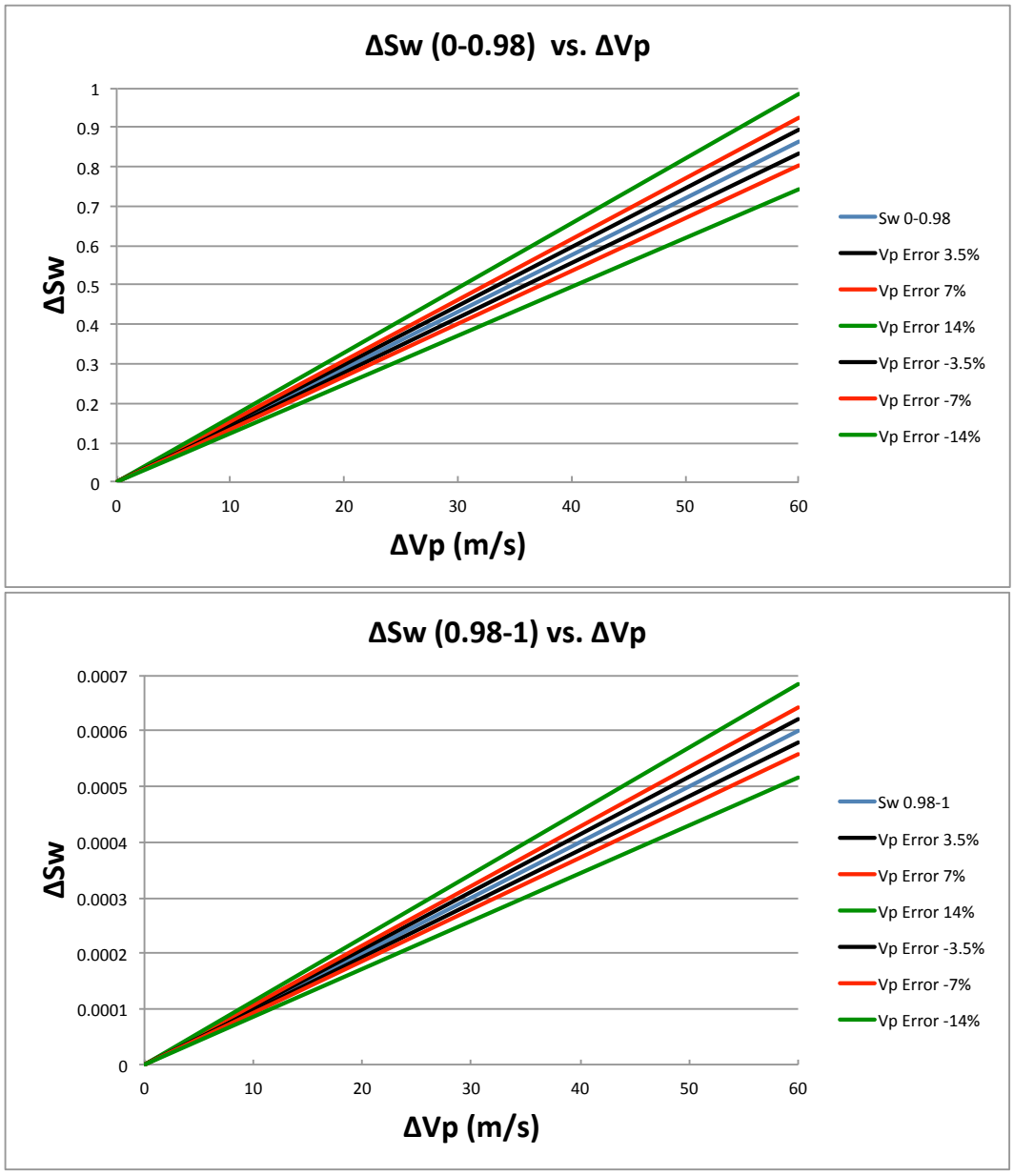


Figure 6.3: Water saturation vs. compressional wave velocity. Plotted above is the change in water saturation vs. the change in compressional wave velocity at 3.5%, 7%, and 14% relative error. There are two graphs, one plots the change in absolute water saturation units from 0-0.98 and the other plots the change in absolute water saturation units from 0.98-1. This is done because there are two separate slopes in when plotting compressional wave velocity vs. water saturation in low velocity sand based on the Biot (1956b, Biot (1956a, Biot (1962) and Gassmann (1951) predictions (Fig. 2.1). The plots show (Fig. 6.3) that as the change in compressional wave velocity increases the change in water saturation increases as well. Where the two slopes converge, at approximately 0.98 water saturation (Fig. 2.1),the change in water saturation vs. the change in compressional wave velocity will go to infinity. This is possible because the relationship between the water saturation and the compressional wave velocity is not linear.

are currently being developed and will be implemented in the years to come.

Other improvements or modifications for the sand tank experiment that are not being currently developed or implemented as of yet include:

- Adding a gravel pack for sand control and increased permeability near well. This would allow the sand tank to be produced at a greater rate therefore decreasing the drawdown time of the well.
- Producing from horizontal wells would increase the production rate and decrease drawdown time for the sand tank. The production calculations for this type of experimental setup would also increase in complexity. This would add complexity to the reservoir simulations as well.
- Having multiple production wells within the sand tank would also lend to interesting experimentation. The well drawdown time would increase, but also, the drainage pattern of the simulations may be interesting.
- Adding and injector well within the sand tank experiment may prove interesting for those interested in enhanced oil recovery (EOR) techniques. This would allow a comparison between EOR calculations of break through time and actual experimental data.

## 6.6 Key Points

- Both the experimental equipment and the theory behind the sand tank experimentation has certain limitations.
- Relative errors associated with the production and seismic data acquisition equipment are within acceptable ranges for this experimentation.
- There are several real world applications for this experiment.
- Several opportunities for future work and improvements to this experiment exist.

# Chapter 7

# Conclusions

The experimental setup in the sand tank is temperamental and, at times, unstable. It is recommended that some of the equipment be replaced or improved. Alternative equipment is needed to provide better measurements in the sand tank experiment. Most notably, a flowmeter that can be calibrated to measure in the correct expected flow range of the sand tank reservoir. If such a flowmeter is used in subsequent sand tank experiments, the accuracy and, therefore the usefulness of the data provided from the experiments would be dramatically improved. Also, a pump that can be more precisely controlled at lower flow rates would be useful in providing more data at different flow rates within the possible low flow range of the sand tank. However, even with the current experimental setup, it was possible to collect quality data for useful experimentation.

The reservoir surveillance equipment in combination with the high frequency seismic data acquisition system for this project is proved to be effective in collecting adequate production and seismic data to allow comparisons to be made between the actual experimental data and calculated data from flow model simulation. The idea of being able to match simulated data to real world experimental data has been realized in the sand tank experimentation. Future experiments that incorporate saturation measurements as well as possible 3-D seismic surveys should prove invaluable in calibrating this sand tank experiment to be used as a closer replica of real world systems.

# Bibliography


Babbage, Charles. 1791-1871. Error Analysis and Significant Figures.

Bachrach, Ran, and Amos Nur. 1998. "High-resolution shallow-seismic experiments in sand, Part I: Water table, fluid flow, and saturation." *Geophysics* Volume 63 (4): pp. 1225–1233 (July-August).

Bear, Jacob. 1979. *Hydraulics of Groundwater*. New York: McGraw-Hill, Inc.

Biot, M. A. 1962. "Mechanics of deformation and acoustic propagation in porous media." *Applied Physics* Volume 33:pp. 1482–1498.

Biot, M.A. 1956a. "Theory of Propagation of Elastic Waves in Fluid-Saturated Porous Solid. I. Higher-Frequency Range." *The Journal of the Acoustical Society of America* Volume 28(2) (March): pp. 179–191.

———. 1956b. "Theory of Propagation of Elastic Waves in Fluid Saturated Porous Solid. II. Low-Frequency Range." *The Journal of the Acoustical Society of America* Volume 28(2) (March): pp. 168–178.

Bommisetty, Ramakumar, Dhanvantri Joshi, and Vighneswara Rao Kollati. 2011, November. "Flow Loss in Screens: A Fresh Look at Old Correlation." *Fluid Power Technology Exhibition*, Volume 3.

Burger, H. Robert, Anne F. Sheehan, and Craig H. Jones. 1992. *Introduction to Applied Geohphysics, Exploring the Shallow Subsurface*. Edited by Leo Wiegman. 500 Fifth Avenue, New York, New York, N.Y. 10110: W. W. Norton and Company, Inc.

Carman, P. C. 1937. "Fluid flow through a granular bed." *Transactions of the Institution of Chemical Engineers* Volume 150:pp. 150–167.

Cerveny, V., I. Molotkov, and I. Psencik. 1977. *Ray method in seismology*. Charles University Press.

Criss, C. J., R. Kappius, and D. Cunningham. 2003, October. "First Arrival Picking Using Image Processing Methods." *2003 SEG Annual Meeting, October 26-31, 2003, Dallas, Texas*. GMG/Axis, Dallas, Texas: Society of Exploration Geophysicists.

Critical Velocity, LLC. 2005-2010. *15 Amp Digital PWM Motor Speed Controller*. 101 West 23rd st number 354 New York, NY 10011: Critical Velocity, LLC.

Darcy, Henry. 1856. “Les fontaines publiques de la ville de Dijon.”

Dupuit, J. 1863. *Estudes Thèoriques et Pratiques sur le mouvement des Eaux dans les canaux dècouverts et à travers les terrains permèables*. Edited by Second. Paris: Dunod.

El-Khamra, Yaakoub Youssef. 2009, November. “Real-Time Reservoir Characterization and Beyond: CyberInfrastructure Tools and Technologies.” Master’s thesis, Louisiana State University.

Fetter, C. W. 2001. *Applied Hydrogeology*. Fourt Edition. Edited by Patrick Lynch. Upper Saddle River, New Jersey 07458: Prentice Hall.

Gassmann, Fritz. 1951. “Elastic Waves through a Packing of Spheres.” *Geophysics* Volume 16(4) (May): pp. 673–685.

Geogiga Technology Corp. 2012. *Geogiga Front End 7.1 User Guide*. 7.1. Sun Life Plaza West Tower 1600, 144-4 Avenue SW Calgary, Alberta T2P 3N4 Canada: Geogiga Technology Corp.

Global Water Instrumentation, Inc. 2006, October. *Water Level Sensor WL400*. 11390 Amalgam Way Gold River, CA 95670: Global Water Instrumentation, Inc.

Horne, Roland N. 1995. *Modern Well Test Analysis*. Edited by Second Edition. Petroway, Inc.

Iotech Inc. 1999-2005. *Users Manual: DaqBoard/3000 Series PCI 16-Bit, 1-MHz Multifunction Boards*. 25971 Cannon Road Cleveland, OH 44146-1833: Iotech Inc.

Johns, Russell T., Larry W. Lake, Rafay Z. Ansari, and Arnaud M. Delliste. 2005. “Prediction of Capillary Fluid Interfaces During Gas or Water Coning in Vertical Wells.” *SPE Journal*, vol. December.

Lake Monitors. 2007. *FreeFlow P-Type Transmitter Installation, Operation and Maintenance Manual*. 8809 Industrial Drive, Franksville, WI 53126: Lake Monitors.

LSU. 2012, February. LSU HPC.

Mavko, Gary, Tapan Mukerji, and Jack Dvorkin. 1998. *The Rock Physics Handbook*. Cambridge University Press.

McMechan, G.A., and W.D. Mooney. 1980. Asymptotic ray theory and synthetic seismograms for laterally varying structures: Theory and application to the Imperial Valley, California.

Meakin, Paul, and Alexandre M. Tartakovsky. 2009. “MODELING AND SIMULATION OF PORE-SCALE MULTIPHASE FLUID FLOW AND REACTIVE TRANSPORT IN FRACTURED AND POROUS MEDIA.” *REVIEWS OF GEOPHYSICS* 47 (July): 47.

Oreskes, Naomi. 2003. *"The Role of Quantitative Models in Science" in Models in Ecosystem Science*. Edited by Charles D. Canham, Jonathan J. Cole, and William K. Lauenroth. Princeton University Press.

Sheriff, R.E., and L.P. Geldart. 1983. *Exploration seismology, volume 2: Data-processing and interpretation*. Cambridge University Press.

Smolkin, David. 2011, May. "Laboratory Scale Seismic Analysis Of A Spatially Variable Hydrological Surface in Unconfined, Unconsolidated Sand." Master's thesis, Louisiana State University.

Stockwell, John W., and Jack K. Cohen. 2008, January. *The New SU User's Manual*. 4.0. Golden, CO 80401, USA: Colorado School of Mines.

Wentworth, C K. 1922. "A scale of grade and class terms for clastic sediments." *Journal of Geology* Volume 30:pp. 377–392.

White, Chris. 2011. Dupuit Graph. Personal Correspondance.

Zelt, C.A., and R.M. Ellis. 1988, June. Practical and efficient ray tracing in two-dimensional media for rapid traveltime and amplitude forwar modeling.

Zelt, Colin. 1988. 2-D traveltime inversion and amplitude modeling programs.

# Appendix A

# Related Computational Tools

## A.1 Super Computer

The software used to process the experimentally collected data in this thesis was all processed on:

Tezpur

[ tezpur.hpc.lsu.edu ]

Tezpur, the university's next supercomputer– named for one of the world's hottest peppers, is a 15.3 TFlops Peak Performance 360 compute node cluster running the Red Hat Enterprise Linux 4 operating system. Each node contains two Dual Core Xeon 64-bit processors operating at a core frequency of 2.66 GHz. Tezpur was delivered to LSU on November 3, 2006 and is open for general use to LSU users (LSU 2012).

- 360 Compute Nodes
- Two 2.66 GHz Dual Core Xeon 64-bit Processors
- 4 GB Ram
- 10 Gb/sec Infniband network interface
- 10/100/1000 Ethernet network interface

- Red Hat Enterprise Linux 4
- 1 Interactive Node
- Two 3.00 GHz Dual Core Xeon 64-bit Processors
- 8 GB Ram
- 10/100/1000 Ethernet network interface
- Red Hat Enterprise Linux 4
- Cluster Storage
- 32 TB Panassas High-Performance disk
- 21 TB GPFS-mounted IBM NSD disk
- PBS Job Management System

## A.2 Software and Programs

- RAYINVR- a program to trace rays in 2-D media for rapid forward modeling and inversion of refraction and reflection travel times written by Colin Zelt (Zelt 1988).

  Program Description: A 2-D (x,z) isotropic medium is assumed. The velocity model is composed of a sequence of layers separated by boundaries consisting of linked linear segments of arbitrary dip. Layer boundaries must cross the model from left to right. Layer thicknesses may be reduced to zero to model pinchouts or isolated bodies. The velocity within a layer is defined by velocity values specified at arbitrary x-coordinates along the top and bottom of the layer. The x-coordinates at which layer boundaries and upper and lower velocities are specified can be completely general and independent within and between layers. Velocity discontinuities across layer boundaries are allowed but not required. For the purposes of ray tracing, the model is automatically broken up into an irregular network of trapezoids, each with dipping upper and lower boundaries and vertical left and right sides. The velocities at the four corners of the trapezoid are used to interpolate a velocity field within the trapezoid so that the velocity varies linearly along its four sides. Therefore, horizontal as well as vertical velocity gradients may exist within a trapezoid. A simulation of smooth layer boundaries is possible in which the incident and emergent ray angles are calculated using the slope of the smoothed boundary. The source(s) may be positioned anywhere in the model and rays may be directed any angle. The receivers are always assumed to be at the top of the model. Both P-

and S-wave propagation can be considered including (multiple) conversions. A unique Poisson's ratio may be assigned to each trapezoid of the model. Refracted, reflected and head waves may be traced, each possibly containing multiple and/or surface reflections and conversions. Ray take-off angles are determined automatically by the program for those ray groups specified by the user using an iterative shooting/bisection search mode. Ray tracing is performed by numerically solving the ray tracing equations for 2-D media, a pair of first order ODE's, using a Runge Kutta method. The ray step length is automatically adjusted at each step to maximize efficiency while maintaining accuracy. Travel times are calculated by numerical integration along ray paths using the trapezoidal rule. A plot of the model and all rays traced may be produced along with a plot of reduced travel time versus distance for the observed and calculated data. The partial derivatives of travel time with respect to those model parameters selected for adjustment are calculated analytically during ray tracing; these parameters include velocities and the vertical position of boundary nodes. The travel times correspond to any ray paths which can be traced through the model, being either first or later arrivals. The travel time residuals with respect to the observed data are also calculated. The travel times and partial derivatives are linearly interpolated to the observed seismogram locations since two-point ray tracing is not required. The partial derivatives and travel time residuals are output and used later as input to the program DMPLSTSQR which updates the model parameters by applying the method of damped least-squares to the linearized inverse problem. The model parameterization is well suited to the inversion of refraction/reflection data since realistic earth models can be represented by a minimum number of model parameters, i.e.,. the number and position of parameters specifying each layer can be adapted to the data's subsurface ray coverage. Layer boundaries, including the surface, may be horizontal (one parameter) or consist of numerous straight line segments. A layer may have a constant velocity (one parameter) or the velocity structure may be defined by many upper and lower layer velocity points. Different velocity points may be specified above and below a layer boundary if a velocity discontinuity is required across the boundary, or a single row of velocity points may be specified if an interface with no discontinuity is needed. The vertical velocity gradient or layer thickness may be fixed in all or part of a layer during the inversion if there is insufficient ray coverage to independently determine an upper and lower layer velocity or layer thickness.

- Geogiga Front End 7.0 - Seismic Data Preprocessing Software

  Geogiga Front End is designed to QC and preprocess single shot record. You can convert data formats, analyze amplitude decay, correct trigger delay, assign geometry, mute seismic traces, run frequency filter, gain control, vertical stacking, and such. Some batch commands are available, such as the geometry assignment, seismic data resampling, and trigger delay correction.

Geogiga Front End is freeware. You are welcome to download, use, and distribute it (Geogiga Technology Corp. 2012).

- The processing of the seismic data was performed with the three programs as mentioned in Smolkin's thesis. For more information on these programs and how to use them refer to the Smolkin (2011) thesis. The three programs are:

    1. des_sandtankstacker.pl
    2. zero.pl
    3. shifter.pl

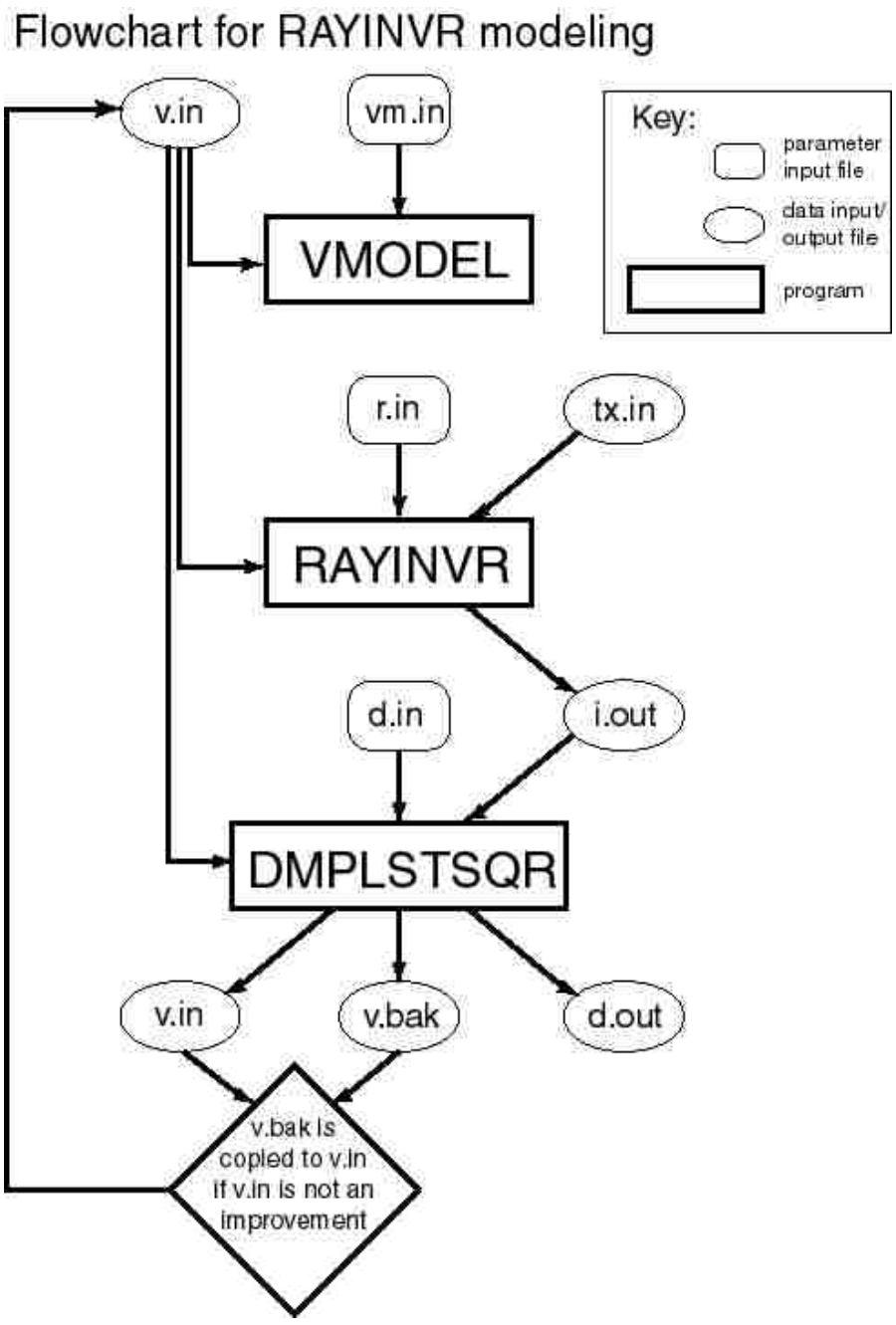


Figure A.1: Rayinvr flow chart

# Appendix B

# Ray Tracing

Derivation of Snell's Law as per Burger, Sheehan, and Jones (1992).

For ray tracing, referring to (Fig. B.1), we can state that the time for a ray to travel from A through some point O to B is

$$t = \frac{(x^2 + y^2)^{1/2}}{V_1} + \frac{((s-x)^2 + y^2)^{1/2}}{V_1}$$

and to determine the minimum value of time t, we can take the first derivative of the function and set it equal to zero

$$\frac{dt}{dx} = \frac{x}{V_1(x^2 + y^2)^{1/2}} - \frac{(s-x)}{V_1((s-x)^2 + y^2)^{1/2}} = 0$$

using the relationships

$$\sin\theta_1 = \frac{x}{(x^2 + y^2)^{1/2}}$$

and

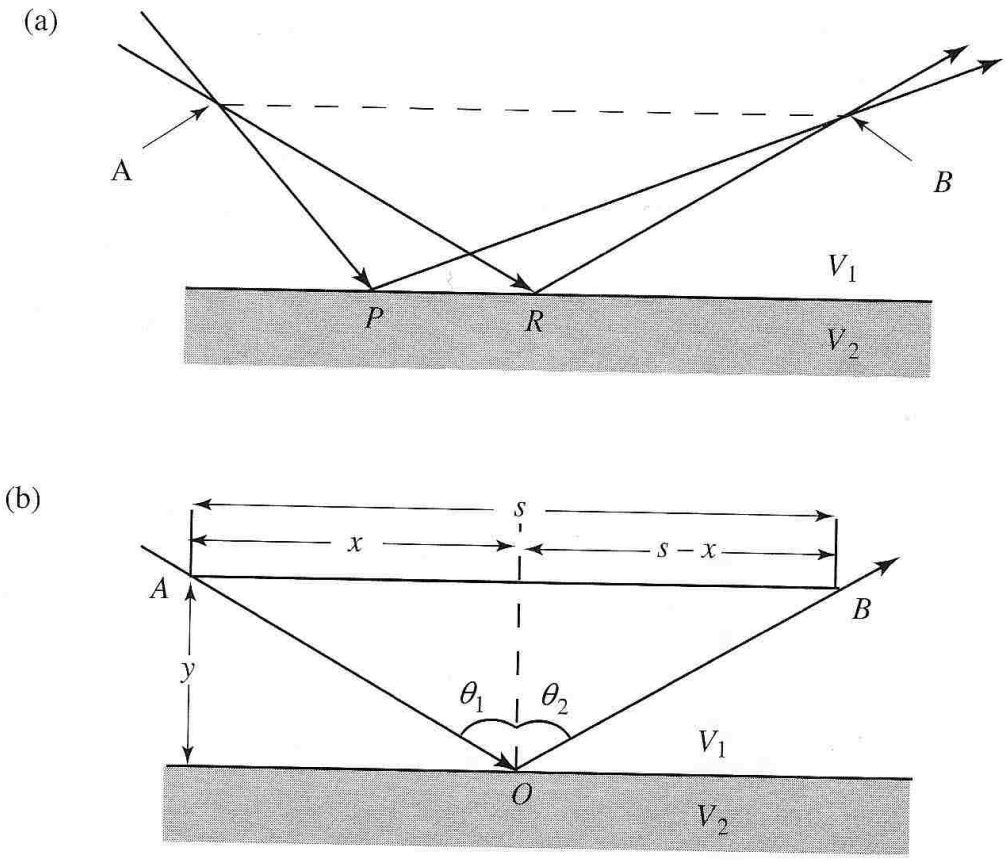


Figure B.1: Fermat's Principle demonstrating that the angle of incidence equals the angle of reflection $\theta_1 = \theta_2$.(Burger, Sheehan, and Jones 1992)

$$\sin\theta_2 = \frac{(s-x)}{((s-x)^2 + y^2)^{1/2}}$$

we can see that

$$\frac{\sin\theta_1}{V_1} - \frac{\sin\theta_2}{V_1} = 0$$

and therefore $\theta_1 = \theta_2$ (Burger, Sheehan, and Jones 1992).

Thus, approaching the geometry of refraction using Huygen's principle (Fig. B.2), we learn that the ratio of the sines of the angle of incidence and angle of refraction is equal to the ratio of the two materials. Once again we can write an equation expressing the time it takes for a ray to travel from A through B to C

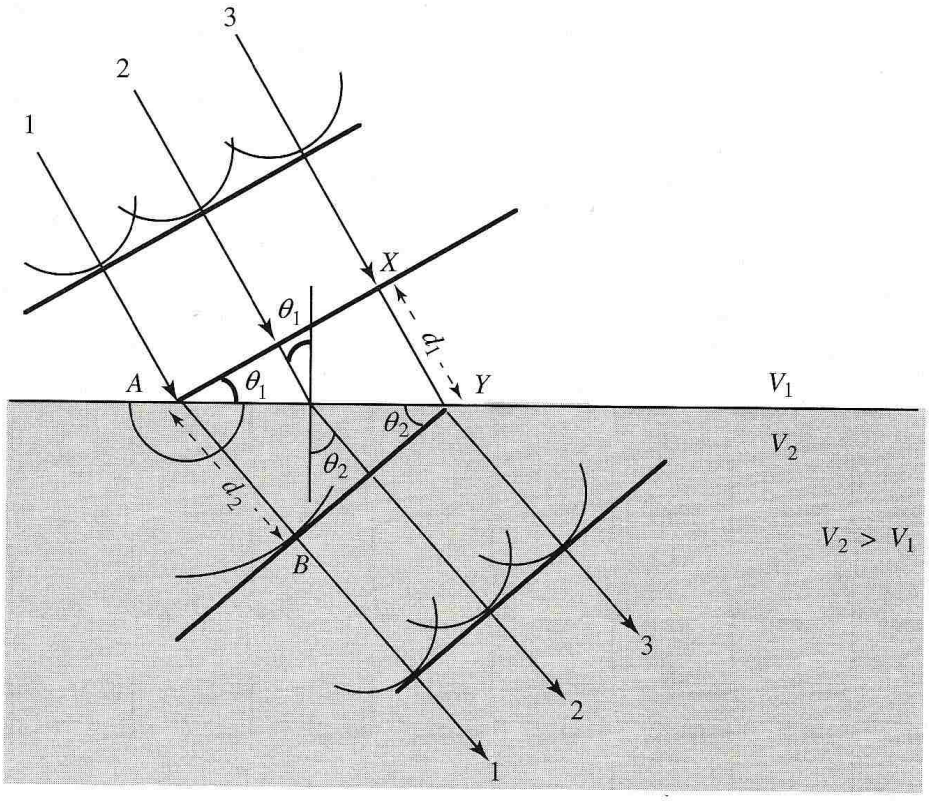


Figure B.2: Huygen's Principle to demonstrate the relationship between the angles of incidence and refraction(Burger, Sheehan, and Jones 1992)

(Fig. B.3).

$$t = \frac{(x^2 + y^2)^{1/2}}{V_1} + \frac{((s-x)^2 + z^2)^{1/2}}{V_2}$$

then taking the derivative and arriving with this expression

$$\frac{dt}{dx} = \frac{x}{V_1(x^2 + y^2)^{1/2}} - \frac{(s-x)}{V_2((s-x)^2 + z^2)^{1/2}} = 0$$

continuing on

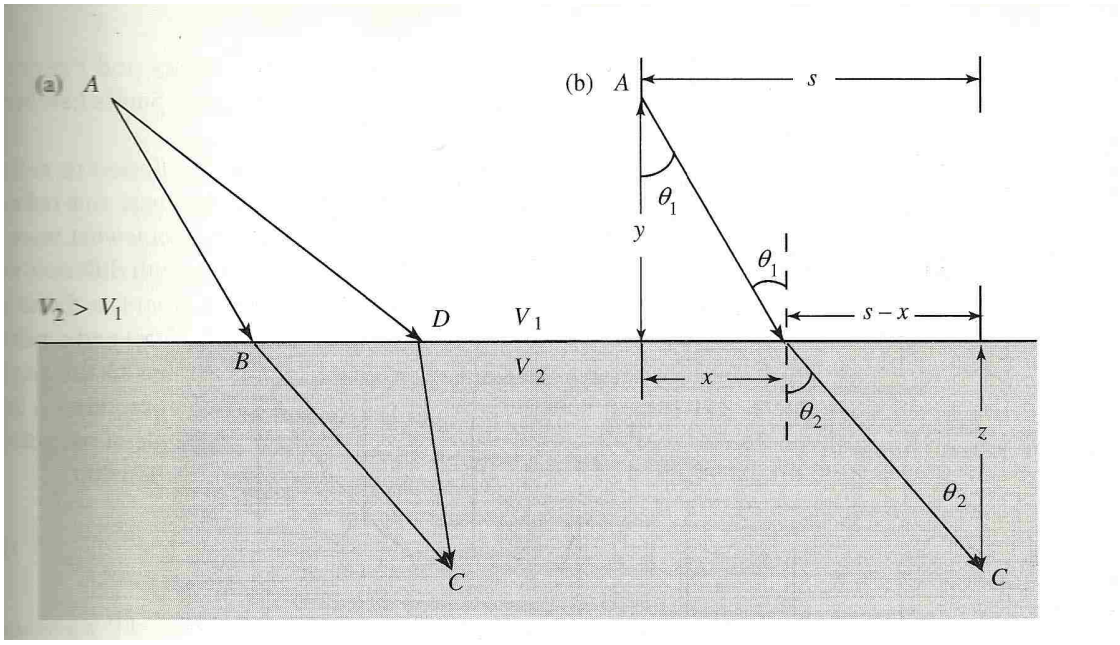


Figure B.3: Fermat's Principle to demonstrate the relationship between the angles of incidence and refraction(Burger, Sheehan, and Jones 1992)

$$\sin\theta_1 = \frac{x}{(x^2+y^2)^{1/2}}$$

and

$$\sin\theta_2 = \frac{(s-x)}{((s-x)^2+z^2)^{1/2}}$$

and then

$$\frac{\sin\theta_1}{V_1} - \frac{\sin\theta_2}{V_2} = 0$$

finally arriving at Snell's Law (Burger, Sheehan, and Jones 1992).

$$\frac{\sin\theta_1}{\sin\theta_2} = \frac{V_1}{V_2}$$

# Appendix C

# Derivation of Chosen Equations

## C.1 Derivation of Dupuit Equation

For unconfined ground water flow Dupuit developed a theory that allows for a simple solution based off the following assumptions:

1. The water table or free surface is only slightly inclined.
2. Streamlines may be considered horizontal and equipotential lines vertical.
3. Slopes of the free surface and hydraulic gradient are equal

The following is a derivation of the Dupuit equation based on the work of Bear (1979).

Darcys law gives one-dimensional flow per unit width as

$$q = -Kh\frac{dh}{dx}$$

At steady state, the rate of change of q with distance is zero, or

$$-Kh\frac{dh}{dx}\frac{d}{dx} = 0$$

$$\frac{-K}{2}\frac{d^2h^2}{dx^2} = 0$$

Which implies that

$$\frac{d^2h^2}{dx^2} = 0$$

Integration yields

$$h^2 = ax + b$$

Where a and b are constants. Setting the boundary condition h = $h_o$ at x = 0, we can solve for b

$$h_o^2 = b$$

Differentiation of $h^2$ = ax + b allows us to solve for a

$$a = 2h\frac{dh}{dx}$$

And from Darcys law

$$h\frac{dh}{dx}\frac{d}{dx} = -qK$$

So, by substitution

$$h^2 = h_o^2 - 2\frac{qx}{K}$$

Setting

$$h = h_L^2 = h_o^2 - 2\frac{qL}{K}$$

Rearrangement gives

$$q = \frac{K}{2L}(h_o^2 - h_L^2)$$

For Petroleum Engineers this would be

$$q = \frac{2\pi kh(p_e - p_{wf})}{\mu B(ln\frac{r_e}{r_w})}$$

In US field units it would be

$$q = 0.00708\frac{kh(p_e - p_{wf})}{\mu B(ln\frac{r_e}{r_w})}$$

Then the general equation for the shape of the parabola is

$$h^2 = h_o^2 - \frac{x}{L}(h_o^2 - h_L^2)$$

However, this does not consider recharge to the reservoir.

# Appendix D

# Pressure Loss Through Production Well

The production flow rates observed in this experimentation are very low in comparison with actual field production flow rates. The flow rates through the slotted PVC are even lower, however, there are still some questions which must be answered.

## D.1 Mean Fluid Velocity

First we must calculate the mean fluid velocity for the flow rates in this experiment.

$$V = \frac{q}{2.448d^2}$$

Where $V$ is the mean velocity in ft/s, $q$ is the flow rate in gal/min, and $d$ is the diameter of the slot in inches. The mean velocity in this experiment is

$$V \simeq 6ft/s$$

## D.2 Flow Regime

Using the equation below we can examine whether the flow in this experiment is laminar or turbulent.

$$N_{Re} = \frac{928\rho V d}{\mu}$$

Where $N_{Re}$ is the Reynolds number, $\rho$ is the fluid density in lbm/gal, $V$ is the mean velocity in ft/s, $d$ is the diameter of the slot in inches, and $\mu$ is the viscosity in cp. When the $N_{Re}$ is less than 2100 it is in the laminar flow range and when $N_{Re}$ is greater than 2100 it is in the turbulent flow range. For this experiment the $N_{Re}$ is

$$N_{Re} \simeq 121$$

which is well below the 2100 mark, thus, the flow in this experiment is laminar.

## D.3 Critical Velocity

Then we must find the critical velocity of the fluid to determine the method with which we can find the discharge coefficients for the slotted PVC. The critical velocity of water can be found as shown below.

$$V_c = \frac{68.1}{\sqrt{\rho c}}$$

Where $V_c$ is the critical velocity in ft/s, $\rho$ is the fluid density in lbm/ft$^3$, and $c$ is the isothermal compressibility of the fluid in psi. For this experiment

$$V_c \simeq 121$$

## D.4 Discharge Coefficient

Since the mean fluid velocity in this experiment is less than the critical fluid velocity, we can use the relation below to compute a discharge coefficient.

$$q = 22800 C_d d \sqrt{\frac{\triangle P}{\rho}}$$

Where $q$ is flow rate in $ft^3/day$, $C_d$ is the dimensionless discharge coefficient, $d$ is the slot diameter in inches, $\triangle P$ is the pressure difference in psi, and $\rho$ is the density in $lbm/ft^3$. Using this relation the calculated discharge coefficient for this experiment is

$$C_d \simeq 1.2$$

This is a reasonable value per research done by Bommisetty, Joshi, and Kollati (2011). For incompressible fluids they found the discharge coefficient, $C_d$, of approximately 0.85 in simulation and 1.4 in experimental work. Shown is a plot of pressure loss vs. flow rate using the calculated discharge coefficient for this experiment (Fig. 4.5).

# Vita

Shannon Ray Chollett was born in Mora, Minnesota, in 1975. He graduated in 1994 from Clarkston High School in Clarkston, Washington. In 2006, after working for a decade, he enrolled at Boise State University in Boise, Idaho. He pursued a Bachelor of Science in Geophysics at Boise State University. While at Boise State, he continued on with his career as an IT Systems Engineer for Supervalu Inc. working on the night shift so he could attend class during the day. After graduating from Boise State in 2009, he began his Master of Science in Petroleum Engineering at Louisiana State University in Baton Rouge, Louisiana. During the summer of 2011, he completed an internship with SM Energy and was later offered a job from Newfield Exploration and Production in Denver, Colorado. In May of 2012, he graduated from LSU with a Master of Science in Petroleum Engineering.